J Mater Sci (2021) 56:1980–2015

Review

Sintering of MAX-phase materials by spark plasma and other methods

J. Lyu[1,*], E. B. Kashkarov[1,*], N. Travitzky[2,3], M. S. Syrtanov[1], and A. M. Lider[1]

[1] Division for Experimental Physics, School of Nuclear Science and Engineering, National Research Tomsk Polytechnic University, Lenin Ave. 43, Tomsk 634034, Russian Federation
[2] Division for Materials Science, School of Energy and Power Engineering, National Research Tomsk Polytechnic University, Tomsk 634050, Russian Federation
[3] Department of Materials Science, Glass and Ceramics, Friedrich-Alexander-Universität Erlangen-Nürnberg, 91054 Erlangen, Germany

Received: 30 July 2020
Accepted: 18 September 2020
Published online: 2 October 2020

ABSTRACT

This review focuses on the comparison of the spark plasma sintering (SPS) with other fabrication methods of MAX-phase materials. In the view of optimizing properties for prospective applications, we summarized different routes to synthesize and sinter bulk/powder MAX-phases with various microstructures, discussed the phase composition of MAX-phases obtained by SPS and other methods. In the article, we introduced the experimental features of various sintering methods and carried out the comparative analysis of "competition phenomenon" between the SPSed MAX-phases and MAX-phases prepared by other technologies. We referred to relevant reports and reviews in which one can acquire a comprehensive understanding of sintering kinetics, sintering thermodynamics, grain growth kinetics, and densification mechanisms. Furthermore, the influence of the sintering routes on the properties of the MAX-phases was discussed paying emphasis on the mechanical properties.

Introduction

The MAX-phase materials is a relatively new class of layered ternary ceramic that is a very active and burgeoning area of research [1]. In 2000, Barsoum published a review article on such ceramic materials and first introduced the concept of "$M_{n+1}AX_n$ phase" (MAX-phase for short) to collectively refer to this type of ceramic material [2]. Among the early MAX-phases, an early transition metal is used as an M element, a *p*-element usually belonging to groups IIIA or IVA in the periodic table is applied as a A component, and X is C and/or N, $n = 1…3$ [3–6]. To date, close to 80 ternary MAX-phases have been

Handling Editor: M. Grant Norton.

Address correspondence to E-mail: czinchzhe1@tpu.ru; ebk@tpu.ru

https://doi.org/10.1007/s10853-020-05359-y

experimentally synthesized, with an overall count of more than 150 MAX-phases, including those predicted by theoretical studies [7]. As seen in Fig. 1, the M elements have been expanded from early transition metals such as Ti, V, and Cr to rare earth elements such as Ce, Pr [8], A elements have also been extended from well-known Group IIIA and Group IVA elements to late transition metals such as Au, Ir, Zn, and Cu [9–11] and B element is added to the group of X elements (for example Ti_2InB_2 [12], V_2AlB [13]).

The study of the electronic structure of MAX-phases reveals that the M-X bond is characterized by a strong covalent bond or ionic bond, which is comparable to their respective MX binaries. The weak covalent bond (similar to the weak van der Waals force between layered graphite) or metal bond between M-X lamellar and plane of A atoms (M-A bond) makes it possible for A atoms break free from the bondage of M-X lamellar. In addition, the metal bond is found to exist between M elements [4, 14–18]. Due to the above unique structure characteristics, MAX-phases differ from traditional ceramic materials and have excellent properties of both metal and ceramic [19]. Like metals, MAX-phases exhibit good electrical and thermal conductivity at room temperature (usually better than the corresponding pure metals) [16]. In addition, MAX-phases are machinable due to the layered structure, tolerant to thermal shock (~ 1400 °C), and demonstrate plastic deformation at high temperatures [17]. In MAX-phases, typical properties of ceramic materials are also exhibited such as being hard and elastically rigid (much higher stiffness than the parent metals), lightweight, corrosion-resistant with high melting points, excellent oxidation resistance, high thermostability, high strength at high temperature, and low expansion coefficient [17, 20]. More meaningful is that MAX-phases have even better self-lubricating properties than graphite [21]. All of the excellent properties of MAX-phases are expected to make them widely used in electromechanical, concentrated solar power (CSP), instrumentation, metallurgy, automotive, marine, aerospace, and other fields as both bulk and thin films/coatings [15, 16, 22–35]. At present, an enormous amount of work about MAX-phases has been carried out, but not limited to, in the area of the research of the synthesis and preparation process of various powders and dense blocks, the preparation of composite materials, and the research of various properties, such as high-temperature oxidation, friction properties, high-temperature self-healing properties, radiation resistance [15, 16]. A good introduction of the MAX-phases is given in several brief overviews [1, 14, 16, 36, 37]. For more information on the MAX-phases and an in-depth overview of their properties, we refer the reader to review articles on Cr_2AlC [38, 39], Ti_2SC [40], Ti_3SiC_2 [41–43], Nb_4AlC_3 [21] and Ti_3AlC_2 [44]. Nevertheless, there has been no systematic comparative analysis of MAX-

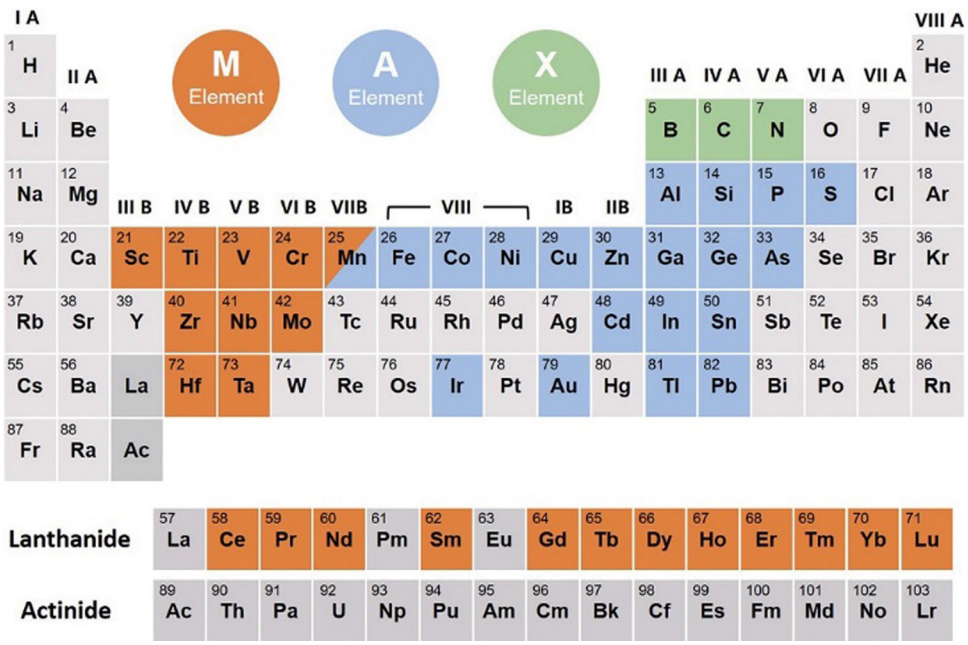

Figure 1 Element distribution of various end-member and solid-solution MAX-phases known to date. The data in the table comes from tables in Refs. [37, 45].

phase materials in terms of various sintering methods.

In the view of optimizing properties for prospective applications, we summarized different routes to fabricate MAX-phase materials with various crystal structures, discussed the phase composition of MAX-phases obtained by spark plasma sintering (SPS) and other sintering methods. We briefly described the experimental processes of various sintering methods, referring relevant reports and reviews in which one can acquire comprehensive understanding of sintering kinetics, sintering thermodynamics, grain growth kinetics and densification mechanisms. Recent developments have revealed the potential of MAX-phases for further application and have led to accessible strategies to sintering new MAX-phases using the SPS and other SPS-based technology.

Processing of bulk MAX-phases

Ceramic materials are usually not manufactured by plastic deformation, mechanical machining or casting but their production involves powders shaping and successive consolidation at high temperatures [23]. This latter process, typically defined as sintering, requires the activation of mass transport mechanisms, which account for the formation of bonding necks between the powder particles, densification, and grain growth. Sintering needs to be carried out at high temperatures to guarantee sufficient atomic mobility and for this reason, it is also often indicated as firing [23]. Two fundamental phenomena take place during sintering: (1) the particles are bonded forming the so-called necks, at the base of which surface diffusion and evaporation/condensation are occurred; (2) the center-to-center particles distance is reduced, thus causing volumetric shrinkage and densification [46]. Corresponding sintering routes of various MAX-phases are presented in the review of Haemers et al. [7], in which one can conclude that pressureless sintering (PLS) is a relatively traditional sintering method, following conventional curvature-driven grain growth [47]. Compared with other sintering methods, PLS is more suitable for industrial-scale production with low cost and simple operation conditions [15]. However, PLSed products have large grain size, low densification, and inferior mechanical properties [7, 38, 40, 48–51]. In addition, for some MAX-phases, such as Cr_2AlC, full densification cannot be obtained by either one-step PLS or two-step PLS without using ultrafine powders. Therefore, pressure-assisted sintering such as hot-pressing (HP), SPS, or hot isostatic pressing (HIP) arises at the historic moment, which promotes the full densification without using ultrafine powders [18]. The quasi-static compressive stress applied during the sintering process leads to better contact between particles, changes the amount and morphology of those contacts, enhances the existing densification mechanisms already present during free sintering (grain boundary diffusion, lattice diffusion, and viscous flow) or activates new mechanisms, such as plastic deformation or grain boundary sliding [52]. With the development of sintering technologies in recent years, it is now possible to sinter MAX-phases with high densification, high purity, and excellent properties. Nevertheless, the sintering of MAX-phases with controlled microstructure, phase composition and properties is still considered the open problem.

HP and HIP

Nowadays, most of the MAX-phases are produced via powder metallurgy routes such as HP and HIP [48, 53–58], which are mature pressure-assisted sintering technologies. The operating characteristics of HP make the compacting pressure only 1/10 of that of cold-pressing and allow reduce the sintering temperature and shorten the sintering time, so as to inhibit grain growth and improve densification and purity without using sintering aids. Although HP is a well-developed method, it has the limitations due to complex processes and equipment, strict requirements for production control and mold materials, high energy consumption, low production efficiency, and high production cost [38]. Further to that, it should be noted that uniaxial pressing used in HP usually leads not only to significant friction between the powders and the mold but also the pressure loss along the pressing direction, so that the density of each part of the compact is not uniform. Different from the uniaxial pressing of HP, during HIP the same pressure is applied on the specimen in all directions by injecting liquids or gases (such as nitrogen and argon) as pressurized media into air-tight vessels with the temperature of 900–2000 °C and pressure of 100–200 MPa [59]. This makes HIP the most widely accepted method of material densification, which allows effectively remove defects and

pores in specimens [60–62]. Furthermore, compared to HP, HIP requires lower sintering temperature and less sintering time [38, 63]. Another advantage of HIP is the ability to prepare ceramics of various sizes and shapes [61].

Since both HP and HIP belong to high-temperature and high-pressure sintering methods, for further understanding of densification mechanisms, including thermodynamics and kinetics of densification of powders by these methods, we refer the reader to Web resources [64–66].

Self-propagating high-temperature synthesis (SHS)

One of the promising fabrication technologies of MAX-phases is SHS [67–69]. In the process of SHS, two or more kinds of powders are mixed and pressed followed by local igniting in the air or protective atmosphere. The heat released from combustion induces the adjacent combustion reaction, forming a self-propagating combustion wave. After the combustion wave passes, new compounds are formed. It is worth mentioning that SHS can be carried out only when the following requirements are met: (1) In general, the continuity of the weakly exothermic reaction cannot be maintained without external energy input. Therefore, the reaction must be high exothermic so that the heat released by the reaction can make the unreacted part reach the combustion temperature; (2) in the process of reaction a reactant should be able to form a liquid or gaseous state, which allows facilitating diffusion and mass transfer so that the reaction can be carried out quickly; (3) the heat loss (convection, radiation, heat conduction) in the reaction process should be less than the increase in the exothermic heat of the reaction, so as to ensure that the reaction is not interrupted [16]. This SHS technique offers several practical advantages [16, 70–74]: (1) Short sintering time. The combustion wave can spread to the entire reaction system in just a few seconds; (2) Low energy consumption. The energy for keeping the reaction process is obtained only from the exothermic heat in the reaction system, and no or only a small amount of external input energy is needed; (3) Small grain size. Because of the fast combustion reaction, large temperature gradient and fast cooling rate, the grain size of the synthesized product is small, and the metastable phase which is difficult to be obtained by other methods can be formed; (4) Low cost. Only a chemical furnace for the self-propagating reaction without a lot of auxiliary equipment is needed. However, due to the short reaction time (fast combustion wave), the rapid cooling rate and the high released energy, which makes SHS a complex multistep process, the reaction process is difficult to control and as a result, some impurity phases in the products are formed, especially in the synthesizing process of solid solution MAX-phases [75–79]. Furthermore, the materials prepared by SHS usually have pores and other defects due to the volatilization of the impurity phase in the reaction process. Despite these drawbacks, compared with thermal reduction and mechanical alloying, SHS still exhibits considerable advantages [41, 70].

To date, SHS technology has made great progress and a theoretical system has been established in the basic theoretical research, including the sintering mechanism, combustion reaction kinetics and thermodynamics, which are present in the review [80] and web resource [81]. Besides, the combination of mechanical activation (MA) and force SHS-pressing technologies has been reported to be expected to obtain compacted samples with higher content of pure phase and more homogeneous structure than that of single SHSed samples [82].

Field-assisted sintering technologies

SPS

Cuskelly et al. [83] classified the production of MAX-phases into two distinct parts of synthesis and shaping (sintering). In the process of traditional PLS of MAX-phases, large pores are generated during the synthesis process due to the lack of assisted pressure to close them hindering the densification of the sample [18]. This hindering effect can be avoided through the two-step process, where the pure phase is first synthesized and the densification process is carried out in a further separate step. Obviously, this will lead to increase in sintering time, especially when PLS is used in both steps [18]. SPS, also known as pulsed electric current sintering (PECS), is a current-activated and pressure-assisted powder sintering technique combining uniaxial HP sintering and plasma activation technology [84–87]. SPS has been firmly incorporated into the laboratory and industrial practice as a one-step method for sintering and

densification of the bulk ceramic samples offering tools to control the microstructure and phase composition of the sintered materials [52, 53, 85, 88, 89]. Similar to HP, as shown in Fig. 2, SPS is often performed when the pressure with maximal loads typically between 50 and 250 kN is applied on the powder compact to enhance densification [52], although pressureless SPS was also investigated [90, 91]. Despite that the SPS process has been deeply investigated [92–95] and widely used for sintering various materials [52, 84, 87, 96, 97], the underlying mechanisms are still not fully understood. It is believed that the complexity of these mechanisms is due to combined mechanical, thermal and electrical phenomena [98]. At present, it is admitted by most research that the complete SPS process follows mainly two stages: (1) Plasma activation. From the punches, the ON–OFF pulse direct current (DC) flows in and through graphite dies and powders. The current, which flows through graphite dies produces a large amount of Joule heat as one of the heating sources of powders. While the current, which flows through the powders, produces plasma as a result of the spark discharge of some gas molecules in the gap between the powers, forming high-speed particles (electrons and positive ions) flow in reverse, which exerts high punch pressure on the surface of particles and thereby blows away the adsorbed gas or broken oxide film as well as purifying and activating the surface of particles. This phenomenon is also known as the electron wind effect [99, 100]; (2) Thermoplastic deformation. As a result of both the discharge heat in the non-contact zone and the Joule heat in the contact zone between powders, a high-temperature field is formed instantaneously. This field leads to melting and evaporation on the surface of the powder particles providing the formation of necks around the contact zone (between the particles) and significantly increases the diffusion of the powder particle atoms. The diffusion coefficient of atoms in this case is much larger than that under the usual hot pressing condition, thereby realizing the quick sintering of powders, reduced sintering time and temperature, and the consolidation of powders without excessive grain growth [100, 101]. Qualitative analysis of the densification mechanism of SPS is performed in reviews [52, 100], where the effect of heating rate, sintering temperature, sintering pressure, pulse current, sintering time, sintering atmosphere, and other parameters are discussed.

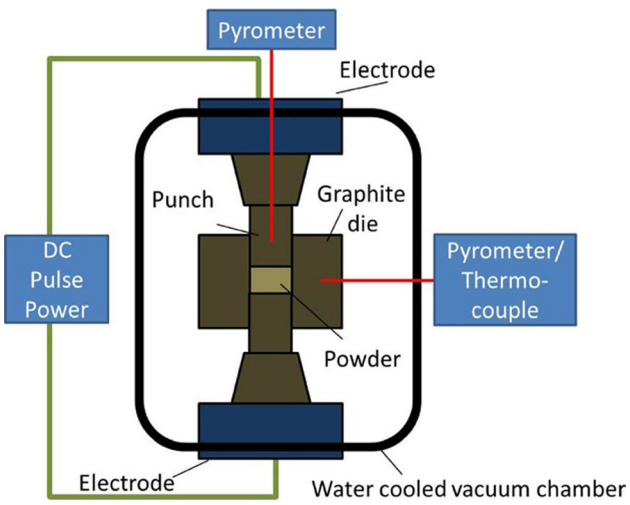

Figure 2 Schematic diagram of an SPS apparatus [52].

Despite some controversy among researchers about the physical processes of SPS, analysis of the literature data indicates that powdered materials, including nanocomposite powders, can be successfully consolidated by SPS into dense materials, which can preserve the microstructure and have novel properties [92, 93, 102, 103]. Compared with the traditional sintering methods, the main advantages of SPS are as follows: (1) Owing to the compact geometry of the die and punches as well as the typical ON–OFF pulse current with the duration in the order of a few milliseconds, the heating process can be controlled with the quick heating rate as high as 1000 °C/min [52, 104]; (2) Plasma-induced surface activation and applied external pressure make it possible to use lower sintering temperature and shorter sintering time to obtain high-density composite materials preserving the small grain size of the matrix [16, 100, 104–108]; (3) The SPS process is binder-less, direct, and cost-effective [16, 38]; (4) The grain size and microstructure of SPS sintered materials can be controlled by adjusting sintering temperature and axial pressure die configuration, etc. [105]. Despite the advantages of SPS among numerous sintering methods, major problems with this perspective technology should not be ignored: (1) Limited by the sintering environment, it is difficult to obtain real-time parameters in the sintering process, which impede accurate analyzation of the sintering process, densification mechanism and influencing factors; (2) Complex power supply equipment and high die cost make it difficult for large scale production [109]. SPS techniques used to be unsuccessful

in preparing compacts with various shapes and big size as almost all the SPS-sintered compacts reported in the literature were cylindrical and their diameters are less than 30 mm [104]. Nowadays, some of these problems can be solved by using new starting materials and graphite tooling production processes. For example, a preceramic paper can be used as a feedstock [110], which is characterized by its properties to be easily shaped into multilayer laminates or more complex shapes [111, 112], and be manufactured in the form of multilayer gradient ceramic composites with enhanced properties. It was reported that the traditionally sintered paper-derived Ti_3SiC_2-based composites have porous structure caused by the long sintering time [113, 114]. This should not be a problem for SPSed paper-derived MAX-phases considering the excellent densification of SPS technology over ceramic materials. The densification process in PL-SPS is the same as the conventional SPS and the transport mechanism is grain boundary diffusion; however, the significant advantage of the former is necking at the early stages [115].

Flash sintering (FS) and flash spark plasma sintering (FSPS)

FS is a novel current-assisted sintering technology developed in the recent years. As shown in Fig. 3, in general, a typical technological process of FS experiment of ceramic can be divided into three stages called constant pressure stage, flash stage and constant current stage [116–119]. Both FS and SPS yielded significant improvements over existing sintering methods, however, the differences between FS and SPS should be noted: (1) In SPS the graphite dies, typically more conductive than the ceramic powder compact, carries the largest part of the electric current [46]. As a result, thanks to good electrical conductivity of the materials used for tooling, low voltages (typically below 10 V applied to the whole set-up) can produce high currents (typically from 1 to 10 kA) leading to efficient Joule heating [52]. Compared to SPS, the current is forced to flow in the ceramic component during a FS experiment. Due to that FS is mainly applied for sintering materials with low electrical conductivity in order to generate significant Joule heating at the constant current stage, and higher applied fields as well as lower current densities characterize the FS process [46, 47]; (2) FS studies are often pressureless [47].

Researchers have done a lot of work on the mechanism of FS process, although there are some common understandings, so far due to the transient nature of FS academia is far from reaching a proven consensus. To describe the FS densification process, the same atomistic mechanisms as for the SPS process, such as spark plasma, local melting and surface softening can also be used [47]. The most significant and appealing mechanisms proposed for explaining the "flash" event including Joule heating effect, thermal runaway theory, the theory of rapid heating promoted densification, grain boundary overheating and mobility, local melting, and Frenkel pairs nucleation have been described in reviews [46, 47, 120, 121]. Also these reviews discussed the influence of processing parameters (i.e., electric field magnitude, current density, waveforms (AC, DC) and frequency, furnace temperature, electrode materials/configuration, externally applied pressure, and sintering atmosphere) on microstructures, densification mechanisms and modeling of FS. Starting from

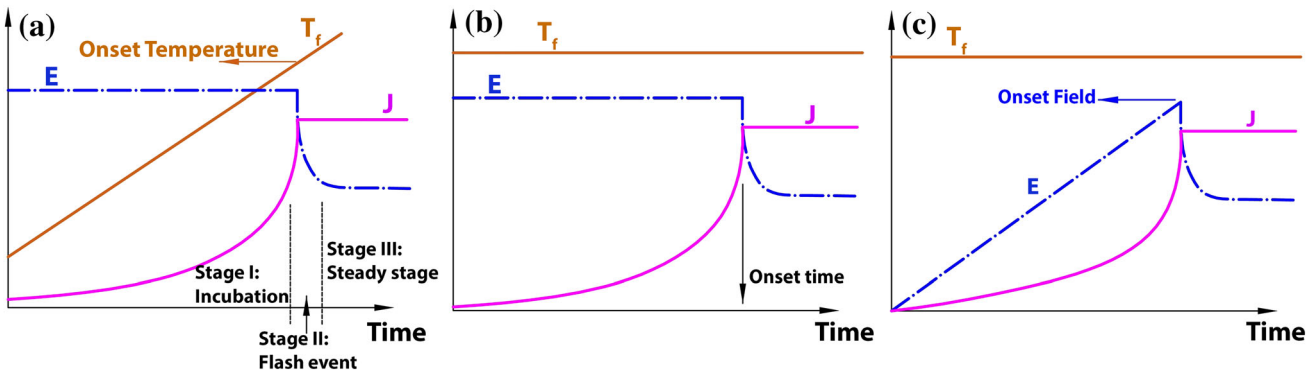

Figure 3 Electric field (E) and current (J) evolution during constant heating rate (**a**) and constant furnace temperature, T_f, (**b**, **c**) flash sintering tests [46].

the prevailing characteristics of SPS and FS over other traditional sintering methods, FSPS [122–126], combining the advantages of both SPS and FS, is recently developed based on the improved commercial SPS platform. Compared with FSPS with no die [127], the power and sintering time can be further reduced with the use of thin graphite die as shown in Fig. 4 [125]. This could be in part explained by the fact that in the early stage of sintering (low-temperature stage), the electrical resistivity of the specimen is high so that the current mainly flows through the die and as a result the specimen is heated by the thermal energy converted from electrical energy with more effective energy utilization than that by furnace heating [120, 125].

It is believed that independent of the sintering method at the same sintering temperature and time the grain growth can be inhibited by higher heating rate [120, 128–135], which facilitates an "out of equilibrium" process and therefore allows to sinter metastable materials or avoid undesired phase transitions. However, it is worth mentioning that in some cases using the high electric field for realizing the higher heating rate may accelerate grain coarsening [136]. This can be possibly explained by the well-admitted theory that in SPS and FS the charged ions at the space charge layer and the point defects at the grain boundary in the applied electric field environment exerts influence on the grain boundary potential. One evidence of the theory is the fact that the majority of the FS experiments were performed with DC due to the directionality of DC field allowing more effective changing the grain growth kinetics during FS [47, 121]. In fact, the influence of the electric field on the sintering process has always been controversial. Based on the experimental fact that regardless of the presence or absence of an electric field, the SHS and FS sintered 3 mol% yttria-stabilized zirconia (3YSZ) specimens demonstrate comparable sintering behavior with similar temperature profiles. Ji et al. [137] believed that the rapid densification in FSed 3YSZ is caused mainly by the indirect effect of the electric field-induced rapid heating rather than any direct effect of the electricity on the net matter transport. Cologna and Raj [138], studying the interaction between the electrical field and neck formation in 3YSZ without reproducing the flash event and Joule heating, concluded that the neck growth rate is substantially unaffected by the field application. On the contrary, Niu et al. suggest that the extremely high-rate densification process achieved during the flash event cannot be explained only by the heating rate itself [125]. Another important point about the mentioned field effect is that the conclusions about the effect of the electric field on a given sintering process may not be suitable for other sintering processed since the type and intensity of electric field are all factors that need to be considered in the study of the field effect. For example, it was believed by Chaim et al. [47] that the AC mode in FS yields finer grain size and more homogeneous microstructures of ceramic nanoparticles. Other researchers analyzed the effect of static electric fields, with no current in the material, on defects generation [139], defect mobility [140], and surface chemistry [141]. Several effects have been theoretically predicted although they appear significant when fields in the order of 10^6 V/cm or larger are applied, which is much larger than the maximum field used upon FS in the order of 10^3 V cm^{-1} [46].

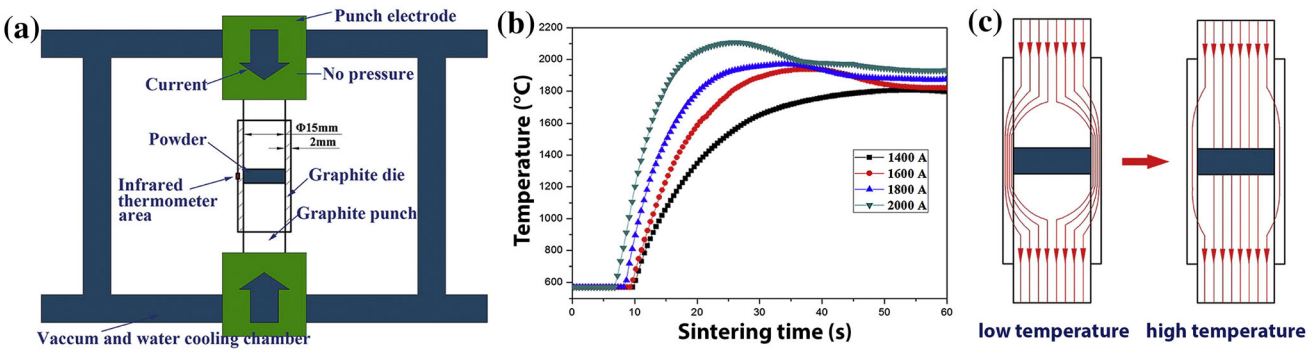

Figure 4 Schematic representation of the FSPS process. **a** Schematic illustration of the graphite die used for the FSPS. **b** Temperature curves versus time during the FSPS processes with different applied currents. **c** Schematic illustration of the current distributions at low and high temperatures during FSPS processes [125].

In recent years, several sintering technologies have also been developed for MAX-phase sintering, such as microwave (MW) assisted SHS [142] and MW + SPS two-step process [143], the densification mechanism of MW is introduced in [144].

Micro-/crystalline structure and phase composition of MAX-phase materials

Micro-/crystalline structure of MAX-phases

The chemical formula of end-member and solid-solution MAX-phases could be generalized as $M_mA_pX_n$ (m, p, and n are integers) [19]. As shown in Fig. 5a [145], when $n = m–p$, $p = 1$, MAX-phases are determined as ternary MAX-phases, crystallizing in a hexagonal structure with $P63/mmc$ symmetry and two formula units per unit cell (UC), which consist of edge-sharing octahedral 'M_6X' octahedra (e.g., Ti_6C) interleaved with layers of A elements (e.g., Si or Ge) [1, 14, 37, 146, 147]. Therefore, A element is also called interlayer element [148]. The grain growth of MAX-phases shows the characteristic of anisotropy (Fig. 5b), therefore, regardless of the sintering methods, the morphology of MAX-phase is generally lath-like [149, 150] or plate-like [151–153]. As can be observed in Fig. 6, many lath-like and layered SPSed V_4AlC_3 phases were distributed at the 3-dimensional directions. In the case of higher magnification one can see in Fig. 6 that the layered V_4AlC_3 is formed along particles pulling out. By increasing the magnification on the lath-like V_4AlC_3 phase, V_4AlC_3 delamination and V_4AlC_3 plastic deformation, which are considered as the inherent properties of MAX-phase could be seen [154]. Furthermore, with reducing the thickness of the formed layer to nano-size the toughness of the prepared sample could be improved. Similarly, the plate-like MAX-phase consisted of a number of thin slices, which were believed to be beneficial for energy absorption when cracking and mechanical property improved, was found in the hot-pressed Ti_3SiC_2 grains as shown in Fig. 7 [153]. According to the n value (stacking number of M-X lamella) in the general formula, MAX-phase can be divided into M_2AX phase (21 l phase), M_3AX_2 phase (312phase) and M_4AX_3 phase (413 phase) [14], the unit cell structures of which are exhibited in Fig. 8. The M_6X structure of ternary layered ceramics is similar to that of MX binary structure, as a result, the ternary layered ceramic material has some physical properties of MX, such as good thermal stability, low coefficient of thermal expansion (CTE), acid and alkali corrosion resistance, good oxidation resistance and so on [16]. As n increases, the properties of these phases become more similar to those of their corresponding binary nitrides or carbides. Thus, the 211 structure with higher repetition of the A-layers has more metallic and better electrical and thermal conducting properties than the 312 and 413 phases that have more carbide- or nitride-like properties [17]. This indicates that the performance of MAX-phase can be controlled by adjusting the thickness of M-X lamellas although it was reported that the stacking number tends to have minimal effect on the intrinsic mechanical behavior of the $Ti_{n+1}AlC_n$ and $Ta_{n+1}AlC_n$ systems [155]. Improved understanding and systematization of how the underlying electronic structure and chemical bonding of MAX-phases affects the macroscopic properties and how they can be tuned were reviewed in [17]. Meanwhile, some MAX-phases with large m/p like Ta_6AlC_5 [156] and Ti_7SnC_6 [157] have been reported.

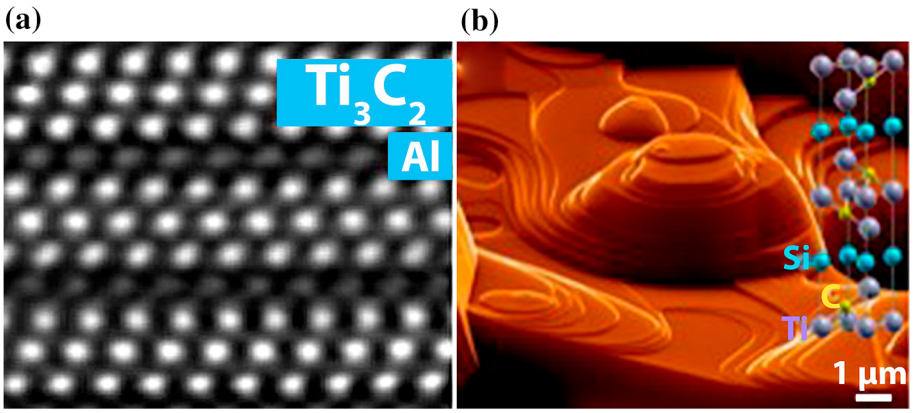

Figure 5 **a** Atomic-scale high-angle annual dark-field scanning transmission electron microscopy images of layered structure of Ti_3AlC_2 along $<11\bar{2}0>$ [145]; **b** crystalline growth inside porous microstructure of Ti_3SiC_2 demonstrating preferred growth in a than c direction [149].

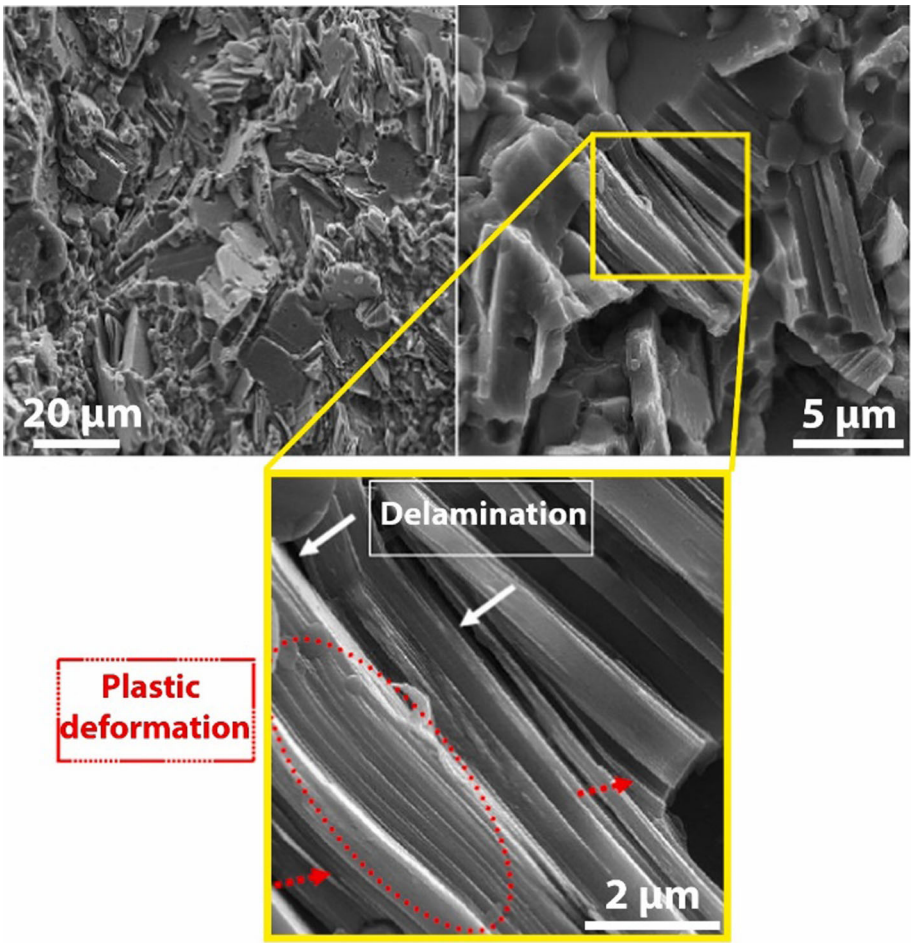

Figure 6 SE-FESEM images of fracture surface of SPSed V_4AlC_3 sample at different magnifications, according to Ref. [150].

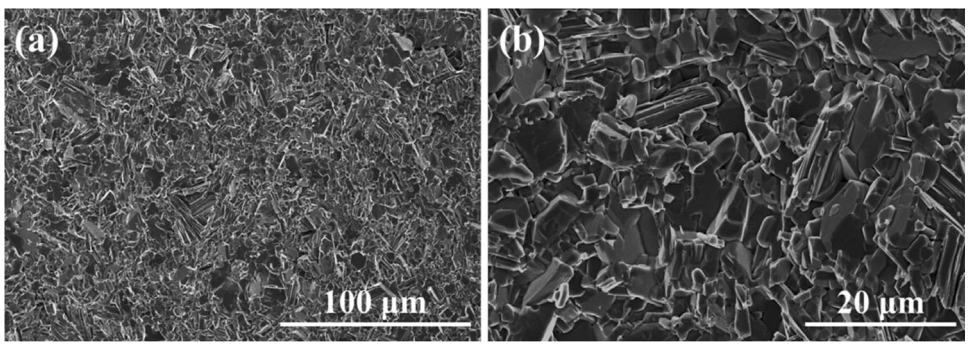

Figure 7 SEM micrographs of the fracture surface of hot-pressed Ti_3SiC_2 ceramic: **a** low magnification; **b** high magnification [153].

When $n = m–p$, p = 1, in addition to end-member MAX-phases solid-solution MAX-phases can also be formed, including chemically random and chemically ordered solid-solution. Most of the chemically solid-solute-random MAX-phases are quaternary MAX-phases, including substitution of M [77, 79, 158–166], A [78, 167–173] and X sites [13, 147]. In addition, a few cases of double solid solutions [174–176] have also been reported. The synthesis conditions of chemically solid-solute-random MAX-phases are not strict since they have been reported to be synthesized by HP [177], PLS [175, 177], SHS [78, 79] and SPS [172]. For chemically solid-solute-random quaternary MAX-phases with the substitution of M site $(M^1, M^2)_{n+1}AlC_n$, because M^1 and M^2 are randomly distributed in the transition metal position, the quaternary MAX-phase retains the *P*63/*mmc* symmetry of the ternary MAX-phases [178]. Different from the substitution of M site, for chemically solid-solute-random quaternary MAX-phases with the

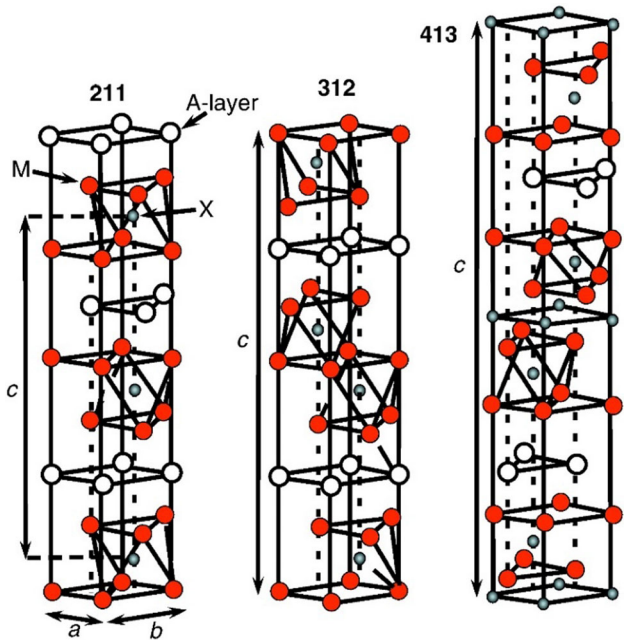

Figure 8 MAX-phase unit cell structures of 211 (n = 1), 312 (n = 2) and 413 (n = 3) [17].

substitution of A site, in addition to the isostructural MAX-phase solid solutions on A site [179, 180], the substitution of A site has also been reported to lead to the symmetry reduction, for example, Nechiche et al. [168] found that the Cu mixing into the Al site of Ti_3AlC_2 is accompanied by lattice distortion, which leads to symmetry reduction from a hexagonal to a monoclinic structure. Such symmetry was attributed to this mixing through the deviation of the A-site position from the special (0, 0, 1/4) position within the $P63/mmc$ space group of the original Ti_3AlC_2 structure. The family of MAX-phases is further expanded by the recent discovery of both quaternary in-and out-of-plane ordered MAX-phases. Unlike chemically random solid-solution, to date chemically solid-solute- ordered MAX-phases can be synthesized only by substituting M site [8, 159, 181–191]. Therefore, the chemically solid-solute-ordered MAX-phases currently only exist in quaternary, which can be classified into in-plane ordered MAX-phases (i-MAX) [8, 181, 183–186, 188–191] and out-of-plane ordered MAX-phases (o-MAX) [159, 182, 187, 188]. In all i-MAX-phases, solid-solute-ordered "211" phases belonging to monoclinic $C2/c$ space group is common, such as $(Zr_{1/3}V_{2/3})_2AlC$ [181], $(Y_{1/3}Mo_{2/3})_2AlC$ [181], $(Sc_{1/3}W_{2/3})_2AlC$ [183], $(Y_{1/3}W_{2/3})_2AlC$ [183], $(Sc_{1/3}Mo_{2/3})_2AlC$ [186], and $(Mo_{2/3}RE_{1/3})_2AlC$ [8], where RE = Nd, Tb, Dy, Ho, Er, Tm, and Lu. The crystal structures of monoclinic $C2/m$ have also been reported to exist in the family of i-MAX-phases, such as $(Mo_{2/3}RE_{1/3})_2AlC$ [8], where RE = Ce and Pr. Furthermore, recently, starting from the DFT theoretical prediction Petruhins et al. [185] sintered two new i-MAX-phases, $(Cr_{2/3}Sc_{1/3})_2GaC$ and $(Mn_{2/3}Sc_{1/3})_2GaC$, crystallizing in an orthorhombic structure ($Cmcm$). While for o-MAX, the solid-solute-ordered "312" phases belonging to the $P6_3/mcm$ space group, such as $(Ti_{1/3}Cr_{2/3})_3AlC_2$ [159, 187] and $(Ti_{1/3}Mo_{2/3})_3AlC_2$ [188], are common. The general formula of o-MAX is $(M', M'')_{n+1}AlC_n$, where M′ (outer layers) and M″ (inner layers) denote early transition metals, occupying different planes (Fig. 9c), and n is either 2 or 3 [37]. The chemical formula for i-MAX is similar to that of the o-MAX-phases, but since n = 1, they are best described as $(M'_{2/3}, M''_{1/3})_2AlC$, where two kinds of M atoms occupy the same plane (Fig. 9b) and the M′:M″ ratio is always 2. In these phases, the M′ atoms are arranged in a hexagonal arrangement, at the centers of which the M″ atoms are positioned [37]. Compared with traditional ternary MAX-phases, most of new higher-order i-MAX and o-MAX-phases have yet to fully establish synthesis routes, thus to date they are prepared superiorly by PLS technique [7, 37, 182].

When $n = m–p$, p = 2 MAX-phases crystallize in $R\bar{3}m$ space group [192], they could be regarded as the stacking-fault-ordered phases or hybrid structures (Fig. 10g) [37]. Currently found stacking forms include …211|312|211|312… and …312|413|312|413 ⋯, which were observed in thin films or bulk samples, such as $Ti_5Al_2C_3$ [192–195], $(V_{0.5}Cr_{0.5})_5Al_2C_3$ [196], $Ti_5Si_2C_3$ [197], $Ti_5Ge_2C_3$ [198], $Hf_5Al_2C_3$ [199], $Ti_7Si_2C_5$ [197, 200], and $Ti_7Ge_2C_5$ [198], This suggests that the performance of MAX-phase ceramic composites is expected to be optimized by preparing MAX-phases with such hybrid structures [14].

Recently, 221 phases such as Mo_2Ga_2C [201, 202], Ti_2Au_2C [203], and 321 phases such as $Ti_3Au_2C_2$ ($P\bar{3}m1$ space group) [9, 203], Nb_3As_2C [204] with $n \neq m–p$, where two layers of A atoms exist between the MX layers, have been synthesized. Furthermore, carbon-vacancy-ordered "413" phases belonging to the $P6_3/mcm$ space group such as $Nb_{12}Al_3C_8$ [205] and $V_{12}Al_3C_8$ [206] have also been reported to exist. The carbon-vacancy-ordered phase belongs to the low-temperature structure in which the contribution

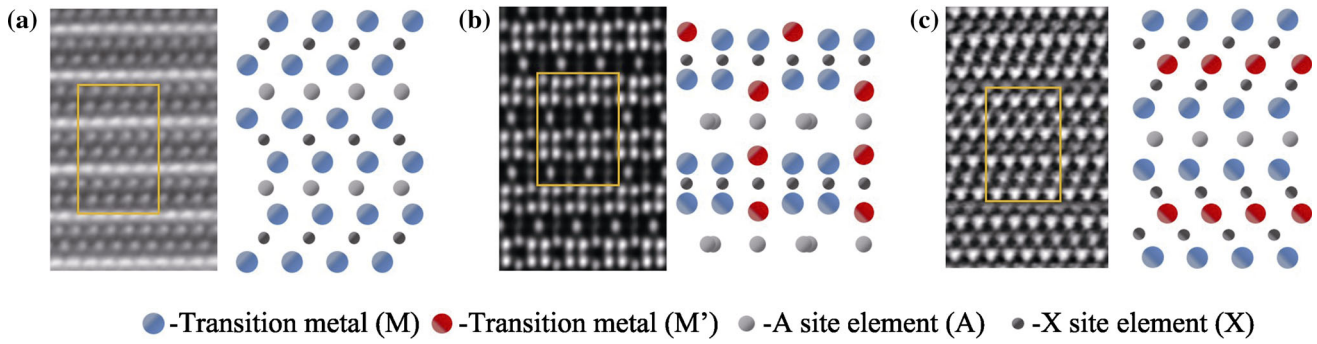

Figure 9 HR-STEM images showing the atomic positions of MAX-phase (**a**), i-MAX-phase (**b**), and o-MAX-phase (**c**) [45].

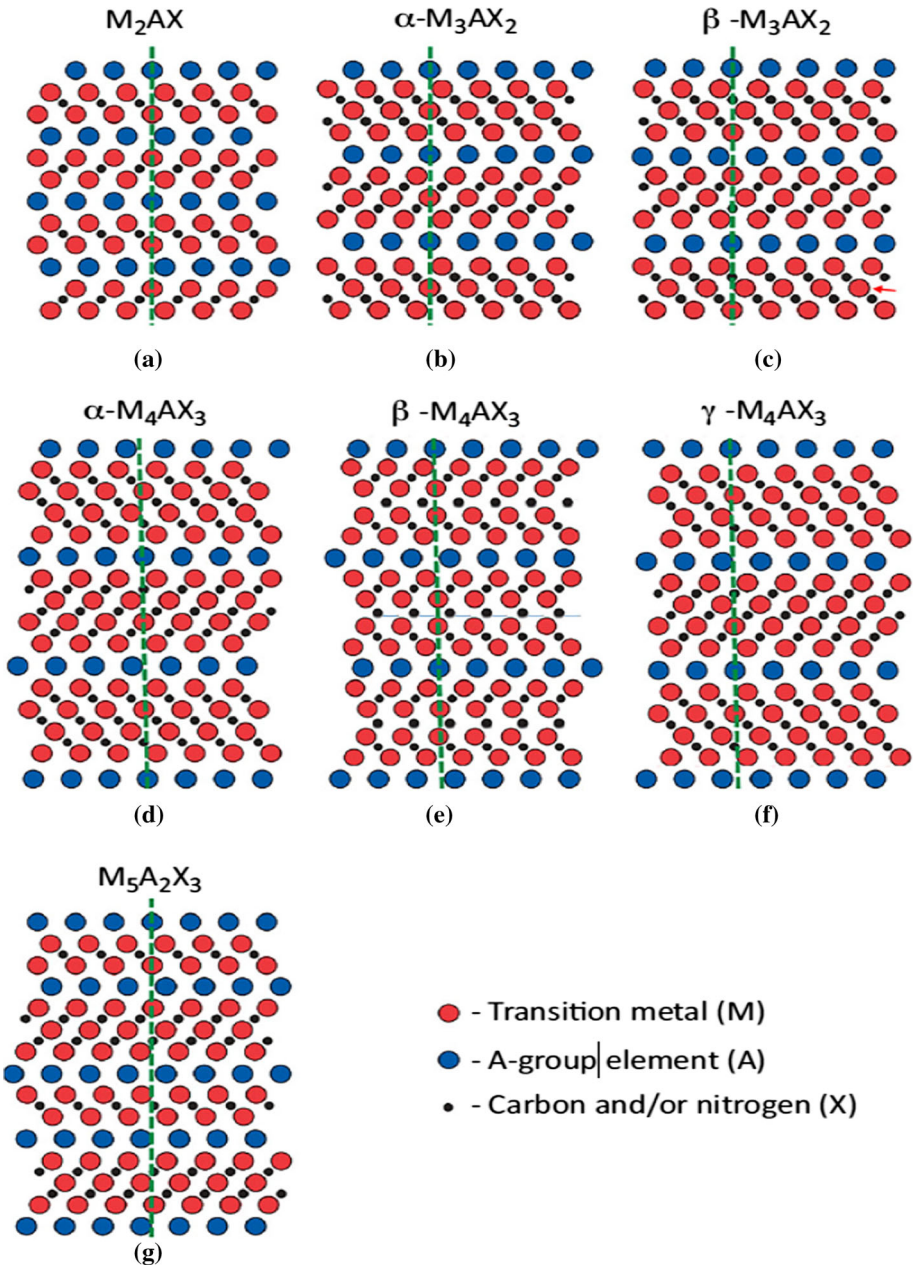

Figure 10 Crystal structures of various MAX-phases. Schematics of the $(11\bar{2}0)$ planes in **a** M_2AX; **b** α-M_3AX_2; **c** β-M_3AX_2; **d** α-M_4AX_3; **e** β-M_4AX_3; **f** γ-M_4AX_3; and **g** hybrid $M_5A_2X_3$ phases. Dashed vertical lines are guides for the eye [37].

of entropy of disorder to free enthalpy increases with temperature [19].

Using only the experimental synthesis method to explore whether a large number of M, A, and X elements can form a stable MAX-phase is very time- and labor-consuming. The method of theoretical calculation allows quickly to explore the unknown MAX-phase system. The ab initio calculations based on Density Functional Theory (DFT) is regarded as a gold standard tool to determine the stability of the MAX-phase by comparing the calculated enthalpy of formation of the MAX-phase with that of the competitive phase in the system. Recently, as shown in Fig. 11, from the calculated formation energies for a very large number of M_2AX phases, it was found that phases containing M = Ti, A = group-13 elements, and X = C constitute the largest number of stable M_2AX phases [207]. It is also believed that solid-solution MAX-phases are more stable than their end-member [207], furthermore, in some cases, solid solutions are stable when one of the end-member is far from being stable [208] or even when neither end-member is [196]. Through evaluation of the stability of o-MAX-phase Mo_2ScAlC_2 using DFT, it was suggested by Meshkian et al. [182] that compared with the chemically disordered solid-solution, chemical order in the quaternary MAX-phase promotes a stable phase. The DFT-based theoretical investigation, conducted by Dahlqvist et al. [209], on the 312 and 413 o-MAX-phases (M′, M′′)AX (M′, M′′ = Sc, Y, Ti, Zr, Hf, V, Nb, Ta, Cr, Mo, W; A = Al; X = C), suggests that the small size difference between M′ and M′′ as well as the large difference in electronegativity between M′ and Al facilitate the formation of o-MAX-phases. Similar empirical design rules for stable MAX compounds, such as choosing A elements of similar radii and M elements of similar valence and electronegativity, have been made for the solid-solution M_2AX phases by Ashton and Hennig [207] through the use of a high-throughput framework coupled to DFT for calculating the formation energies of the 10530 M_2AX compositions. Unlike M and A sites, no significant relationships between the X sites and the formation energy were found by Ashton and Hennig [207]. This is consistent with the findings of [210], which exhibit that despite the slight increase of the total crystal energy due to the reduction in the number of valence electrons and the emergence of weaker Ti–B bonds in the structure of $Ti_3AlC_{2-x}B_x$ ($0.5 \leq x \leq 2$) composition, the structure of the composition system remains thermodynamically stable with the total crystal energy negative up to the complete substitution of carbon atoms with boron atoms. It was also suggested by Burr et al. [211] that $(M, M')_{n+1}AX_n$ MAX-phases with the layered ordering of M on 2*a* sites and M′ on 4*f* sites are expected to exhibit increased stability due to the formation of strong M′–C bond.

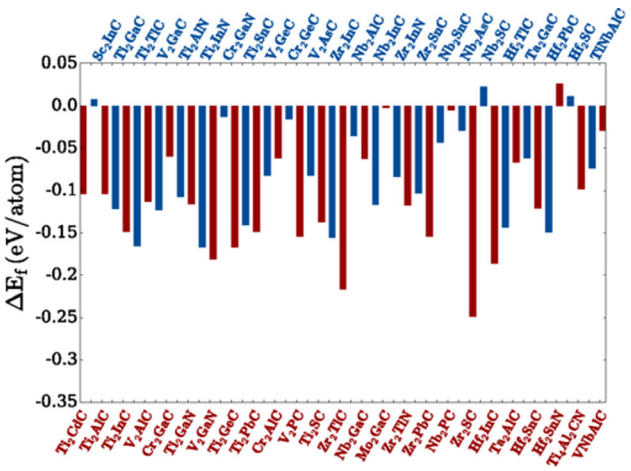

Figure 11 Calculated formation energies for the 49 experimentally known M_2AX phases. Negative (stable) or small positive (slightly unstable) formation energies are predicted for all 49 compounds, with Hf_2SnN showing the highest metastability of 26 meV atom^{-1} [207].

However, Chen et al. [212] believed that only the ab initio calculations based on DFT cannot obtain the complete information about the stability of MAX-phases due to that only the results under 0 K are obtained, which is very different from that of the actual synthesized MAX-phase. In order to predict the stability of MAX-phases at various temperatures, the authors have developed the CALPHAD (Calculation of Phase Diagrams) approach coupled with ab initio calculations. Using this novel calculation approach the authors obtained the thermodynamic stability of Ti_2AuC, Ti_2IrC, Ti_2ZnC, Ti_3AuC_2, Ti_3IrC_2, and Ti_3ZnC_2 at 550 and 1300 °C and confirmed thermodynamic stabilities of the synthesized Ti_3AuC_2, Ti_3IrC_2, Ti_3ZnC_2, and Ti_2ZnC MAX-phases, which is in great agreement with the experiment information. It was interesting to note that these two temperatures (550 and 1300 °C) correspond to the typical temperatures of the molten salt method and HIP in the MAX-phase preparation process, respectively, which suggests the prospect of this novel theoretical calculation approach for obtaining the

stability of MAX-phases depending on the temperature, thereby guiding the selection of sintering methods and adjustment of the sintering temperature in order to experimentally synthesize and sinter new MAX-phases [212].

Phase composition of synthesized/sintered MAX-phase materials

Shamsipoor et al. [53] prepared SPSed Cr_2AlC under different sintering temperatures (1000–1300 °C) and found that high sintering temperature allows increasing the amount of displacement, thereby accelerating the densification process. However, the increment of SPS temperature did not considerably increase the content of Cr_2AlC phase. The densification process can also be accelerated in the case of small particle size of milled powder, which allows increasing the activation energy of milled powder, significantly decrease the enthalpy and Gibbs free energy of reactions and can be obtained by extending ball milling time. It should be noted that in the case of long-term ball milling, impurities such as Fe may appear in the powder when using steel balls [53]. For this reason, the maximum milling time used was only 8 h. The fact that stoichiometric ratio of starting materials plays an important role in the synthesis of MAX-phases is generally accepted in the literature from which we can draw the conclusion that in order to obtain pure MAX-phase, it is necessary to ensure the absolute accord between the molar ratio of actually reacted elements with the stoichiometric ratio of desired MAX-phase. In the work of Shamsipoor et al. [53], the excess amount of Al powder was used in order to compensate for the evaporation of Al from the system during the ball milling and sintering process, which could be accelerated in the vacuum condition of SPS [213]. This reveals the "competition phenomenon" between the high purity and the high densification controlled by the sintering temperature. On the one hand, higher temperatures allow faster diffusion process and movement of atoms, thereby leading to lower porosity and higher density in specimens; on the other hand, due to the various melting points of starting materials, higher temperatures may result in the evaporation of the element with low melting point (for example, aluminum), which exerts negative influence on the sintering process leading to the formation of undesired phases [53, 177]. Furthermore, the high tendency of aluminum for oxidation and the presence of the oxide layer on the surface of Al powders also exhibit the necessity in the isolation of samples from oxygen and the use of excess Al in the process of milling activation and sintering [213, 214]. Thus, although the nominal stoichiometric ratio of Cr:Al:C should be 2:1:1 for the fabrication of Cr_2AlC, the addition of Al should be slightly higher than 1, especially in the long process of common PLS techniques [18, 115, 215]. The same problem was also observed in the SHSed Cr_2AlC from $CaCrO_4 + Al + C$ powder mixtures when the formation of gaseous products (CO, CO_2, Al(g), AlO, and Al_2O) caused a deficiency in these elements in comparison with the stoichiometric composition. This leads to the fact that the formation of the chromium aluminide Cr_5Al_8 and the lower carbide Cr_7C_3 instead of the higher chromium carbide Cr_3C_2 cannot be avoided without adding the excess (superstoichiometric) carbon to the starting mixture [75, 76, 216], which can also explain the formation of secondary phase Cr_7C_3 in the SPSed Cr_2AlC composite in the research work [18, 53]. In contrast to SHSed Cr_2AlC, the significant loss of Al was observed in the SHSed Ti_3AlC_2 from elemental titanium, aluminum, and carbon (graphite) powders, which leads to the formation of the higher titanium carbide by-product TiC [217]. Although based on the experimental results of hot-pressed Ta_2AlC [218] and V_2AlC [219] it has been proposed that the decrement of carbon, i.e., less than 1, is verified to be beneficial for the fabrication of high pure M_2AlC phases, in the case of Cr_2AlC the fact that a deficiency in carbon may increase the risk of formation of the Cr–Al compounds cannot be ignored. The rare successful example for the above-mentioned proposition applied for Cr_2AlC is the SPSed Cr_2AlC in the work of Ge et al. [115] with strict conditions for molar ratios of starting materials, sintering temperature, and holding time. The disappearance of the Cr–Al compounds in the Cr_2AlC sample may arise from the C-uptake from the graphite dies [220], i.e., the Al-volatilization, C-uptake from the graphite dies and the carefully adjusted starting composition (Cr:Al:C = 2:1.3:0.9) leads to complete stoichiometric synthesis of Cr_2AlC. SEM image and XRD analysis results revealed that 1:1.9:1 Ti/TiC/Al powders (i.e., Ti:Al:C = 2.9:1:1.9), activated by ball milling, allow preparing 100% pure Ti_3AlC_2 by HIP technology [221]. This suggests that the molar ratios of starting materials should be selected according to the

conditions of the sintering technology in order to prepare MAX-phases with high purity. However, this selection can be significantly difficult for some MAX-phases, such as Ti_3SiC_2, as the purity of synthesized MAX-phases is very sensitive to the molar ratios of starting materials [172].

As mentioned in "SPS" section is characterized by its fast heating rate, which can inhibit the grain growth of MAX-phases. However, based on the analysis results of XRD and SEM of SPS sintered Cr_2AlC, several authors have shown that the fast heating rate as well as the short holding time are often the limiting factor in the formation of pure MAX-phases [18, 222]. Gonzalez-Julian et al. [18], using elemental constituents Cr:Al:C = 2:1.1:1 and SPS with heating rate 100 °C/min. and holding time 10 min, prepared highly dense Cr_2AlC with secondary phases. Gonzalez-Julian et al. [18] attributed the formation of the secondary phases to the fast heating and the short time, which limited the reaction kinetics to form Cr_2AlC or other intermediate specimens thereby hindering the formation of the pure phase. In contrast, Ge et al. [115], using four different molar ratios of Cr, Al, and C as precursors, synthesized Cr_2AlC phases by PL-SPS and investigated the effect of synthesis parameters on the purity via XRD. The XRD results revealed that in the case of Cr:Al:C = 2:1.3:0.9 and heating rate 100 °C/min the purity of Cr_2AlC increases first and then decreases with the increase of temperature (700–1450 °C) and holding time (0– 30 min), the pure homogenous and porous Cr_2AlC appears at 1300 °C for 15 min, indicating higher decomposition ratio of Cr_2AlC at high temperature with the enlarged cracks and gaps observed in the laminated structure and the increased proportion of other phases. Comparing the works of Ge et al. [115] and Gonzalez-Julian et al. [18], one can conclude that the purity and the density of MAX-phases can be adjusted by the molar ratios of starting materials, heating rate, holding time, and the assisting pressure, that is the high heating rate and high assisting pressure should be applied for high densification of MAX-phases, while for synthesizing MAX-phases with high purity, smaller assisting pressure and longer holding time should be considered first. This conclusion reveals another "competition phenomenon" between the high purity and the high densification controlled by the assisting pressure and can be partly backed up by the evidence in [18], where pure Cr_2AlC bulk materials but with low density were sintered by in situ PLS, and furthermore suggests the application prospect of the two-step process. Instead of PLS, Hamm et al. [143] performed MW heating for synthesizing single-phase V_4AlC_3 as the first step followed by the SPS post-treatment and evaluated the purity of the obtained products by powder X-ray diffraction analysis. The results demonstrate the ability of the MW heating for synthesizing a nearly single-phase V_4AlC_3 product, which was obtained after 60 min of MW heating at 1000 W. Rietveld refinement of the X-ray diffraction data showed that the SPS post-treated composition consists of roughly 98 wt% V_4AlC_3 and 2 wt% VC. The introduction of MW technology into the two-step process is expected to improve the preparing efficiency of MAX-phases with high purity and densification compared with the PLS-contained two-step process. In addition to SPS, HIP can be expected to be an option for the second step (densification/sintering step) in the two-step process due to the applied uniform pressure from all directions. Important note concerning the two-step process must be made here regarding the sintering temperature, high value of which may cause the decomposition of MAX-phase, thereby reducing the purity of MAX-phase. Kozak et al. [223] performed XRD phase analysis of MAX-phase composites based on Ti_3SiC_2 obtained by two-step process (SHS-synthesized powders + HP). It was found that the amount of Ti_3SiC_2 in the SHS-synthesized powders with the average grain size of 8 μm and 20 μm decreases from 75.3 wt% to 52.2 and 61.3 wt% after HP sintering (1500 °C, 25 MPa, 1 h), respectively. Details of the investigation results of the part of the above-selected works on microstructure and phase composition of MAX-phases synthesized by different sintering methods are presented in Table 1.

Mechanical properties of MAX-phases

The layered structure and unique chemical bonding characteristics determine the mechanical properties of MAX-phases, such as higher elastic modulus, strength, and fracture toughness, which arise from the strong M-X covalent bond, while lower shear modulus and hardness, which arise from the weak interaction between M-X layer and A atomic layer [14]. In the case of weak bonding between the A atom layer and M-C layer in the crystal structure, such as

Table 1 Microstructure and phase composition of MAX-phases synthesized by different sintering methods

Sintering method	The parameters of the starting materials			Ball milling parameters		
	Average particle size of raw powders (μm)	Molar ratios of starting materials	Ball to powder mass ratio	Rotation speed (rpm)	Milling time (h)	Ball milled particle size (μm)
PLS in situ	Cr = 26.45; Al = 9.05; C = 6.85	Cr:Al:C = 2:1.1:1	–	150	1/3	–
PLS 2steps	–	–	–	–	–	Pure Cr_2AlC obtained by PLS in situ above = 9.21
SPS in situ	Cr = 26.45; Al = 9.05; C = 6.85	Cr:Al:C = 2:1.1:1	–	150	1/3	–
SPS 2steps	–	–	–	–	–	Pure Cr_2AlC obtained by PLS in situ above = 9.21
SPS	Al = 4; Cr < 250	Cr:Al:C = 2:1.1:1	10:1	250	2	–
SPS	Al = 4; Cr < 250	Cr:Al:C = 2:1.1:1	10:1	250	2	–
SPS	Al = 4; Cr < 250	Cr:Al:C = 2:1.1:1	10:1	250	8	–
SPS	Cr = 20; Al = 40000; C = 15000	Cr:Al:C = 2:1.3:0.9	–	–	–	–
Carbosilicothermic reduction	TiO_2 = 0.2; SiC = 5; Si = 50	TiO_2:SiC:Si = 1:1.2:0.6	–	–	–	–
SPS	V = 250 mesh(58 μm); Al = 250 mesh(58 μm); C < 30 μm	V: Al: C = 2:1.5:1	–	–	1/6	–
SHS	Ti < 40; Al < 60; C < 50	Ti:Al:C = 3:1:2	10:1	–	1	–
SHS	Ti < 40; Al < 60; C < 50	Ti:Al:C = 3:1:2	10:1	–	1	–
SPS	–	Ti:TiS_2:TiC = 1:1.2:1.8 (i.e., Ti:S:C was set as 2:1.2:0.9)	–	200	12	–
HIP	Ti = 45; Al = 45–150; TiC = 2	Ti:TiC:Al = 1:1.9:1	–	–	1	–
HIP	Ti = 45; Al = 45–150; TiC = 2; Sn = 45	Ti:Al:Sn:TiC = 1:1:0.2:1.8	–	–	1	–

Sintering method	Sintering process parameters				Microstructure characteristics		Ref.
	Heating rate (°C min^{-1})	Pressure (MPa)	Temperature (°C)	Holding time (min)	Bulk density (relative density), g cm^{-3} (%)	Phase composition	
PLS in situ	5	Uniaxially precompacted at 200 MPa (green body)	1400	180	3.35 (64.1)	Pure Cr_2AlC with a low concentration of Al_4C_3	[18]
PLS 2steps	5	Uniaxially precompacted at 200 MPa (green body)	1250	180	4.61 (88.1)	Pure Cr_2AlC	[18]
SPS in situ	100	Uniaxially precompacted at 50 MPa for 60 s + 50 MPa in sintering process	1300	10	5.06 (96.8)	Cr_2AlC with small amount of Cr_7C_3.	[18]

Table 1 continued

Sintering method	Sintering process parameters				Microstructure characteristics		Ref.
	Heating rate (°C min^{-1})	Pressure (MPa)	Temperature (°C)	Holding time (min)	Bulk density (relative density), g cm^{-3} (%)	Phase composition	
SPS 2steps	100	Uniaxially precompacted at 50 MPa for 60 s + 50 MPa in sintering process	1250	10	5.17 (98.9)	Pure Cr_2AlC (with a low concentration of Cr_2Al, which were not detected by XRD but were detected by SEM)	[18]
SPS	100	30	1000	30	5.04	Cr_2AlC(64.17 wt%); Cr_7C_3(37.15 wt%)	[53]
SPS	100	30	1300	30	5.21	Cr_2AlC(68.05 wt%); Cr_7C_3(31.95 wt%)	[53]
SPS	100	30	1100	30	5.18	Cr_2AlC(97.24 wt%); Cr_7C_3(2.76 wt%)	[53]
SPS	100	–	1300	15	Porous	Pure Cr_2AlC	[115]
Carbosilicothermic reduction	100/3	–	1600	360	–	Ti_4SiC_3 (92 vol%); TiC(2 vol%); Ti_3SiC_2(6 vol%)	[152]
SPS		10 MPa (with increasing the temperature) and 30 MPa (at the temperature of 1350 °C)	1350	–	(99.1)	V_2AlC (domin phases); Al_2O_3 (a slight amount)	[213]
SHS		Wave propagation synthesis (reaction chamber)			–	Ti_3AlC_2(60 wt%); TiC (40 wt%)	[217]
SHS		Thermal explosion synthesis (tubular furnace)			–	Ti_3AlC_2(85 wt%); TiC (15 wt%)	[217]
SPS	50	–	1450	10	4.3(93)	Ti_2SC with high purity	[220]
HIP	–	Under the argon pressure of 50 MPa for 1 h.	1450	120	–	XRD rietveld refinement: 100 vol% Ti_3AlC_2; SEM image analysis: 100 vol% Ti_3AlC_2	[221]
HIP	–	Under argon pressure of 50 MPa for 1 h.	1450	120	–	XRD rietveld refinement: 100 vol% $Ti_3Al_{0.8}Sn_{0.2}C_2$; SEM image analysis: $Ti_3Al_{0.8}Sn_{0.2}C_2$ (97.82 vol%) + Ti_xAl_y(2.18 vol%)	[221]

Nb_4AlC_3, the formation and slipping of dislocations can be easily generated, which induces the formation of kink bands in the grains presenting "quasi-plastic" behavior [224]. In addition, the dislocations as result of the layer slipping may lead to plastic deformation [15, 149]. It can be seen from Figs. 12 and 13 that different sintering methods can cause variation in grain sizes of the prepared MAX-phase due to different heating rates, holding time, and other characteristics, which thereby exert an influence on mechanical properties [222, 225, 226].

It has been widely admitted that the coarse-grained MAX-phase materials demonstrate higher fracture toughness compared to fine-grained due to the deflection and delamination of cracks by single grains, as a result of which profusion of crack bridging processes in the crack wake occurs (Fig. 14a) [226–228]. Thus, for MAX-phases with high fractured toughness the choice of SPS technology is not suggested or at least should be considered carefully. In addition, it has also been suggested that grain size of MAX-phases exerts a significant influence on the possibility of grains to kink (Fig. 14b [229]): the larger is the grain size, the easier is the kink formation [230, 231]. It is worth mentioning that since kinking is a form of plastic buckling, the lack of constraint, due to increase in porosity which leads to reduction of the threshold stresses needed for incipient kink band formation, must facilitate the formation of more incipient and regular kink bands [229, 232]. Therefore, more kink bands can be predicted to be produced in the PLSed MAX-phases than in the MAX-phases sintered by SPS and other pressure-assisted sintering technologies. Another interesting phenomenon related to porosity lies in the inverse relationship between flexural strength and porosity (proportional relationship between flexural strength and density), which is backed up by the evidence in Ref. [113]. In this work, a more than fivefold increase in the flexural strength of paper-derived Ti_3SiC_2 was observed as a result of preceramic paper densification by calendering. Parrikar et al. investigated the influence of microstructure on the mechanical response of the dense Ti_2AlC processed by reaction sintering [233] and PLS + SPS two-step process [225]. It was found that the grain growth leads to a decrease in the temperature of failure and a correlation with the Hall–Petch relation between compressive strength and grain length was observed. Lapauw et al. [234] found that grain size coarsening of $(Nb_{0.85},M_{0.15})_4AlC_3$ with M = Ti, Zr and Hf in the case of M = Zr lead to the slightly lower room temperature flexural strength of $(Nb_{0.85},M_{0.15})_4AlC_3$ (~ 490 MPa) compared with that of Nb_4AlC_3 (573 MPa).

The effect of grain size on the creep behavior of MAX-phase was reported by Radovic et al. [235, 236] based on the experimental investigation on tensile creep of coarse-grained and fine grained (3–5 μm) Ti_3SiC_2 in the 1000–1200 °C temperature range. It was found that the coarse-grained Ti_3SiC_2 exhibited lower creep rates and longer times to failure than their fine-grained (3–5 μm) counterparts. The longer times to failure of the coarse-grained Ti_3SiC_2 were explained by the authors considering the ability of the larger grains, the basal planes of which are normal to the applied load, to form tenacious crack bridges by delamination and kink band formation, in addition to the bridges that occur when the basal planes are parallel to the applied load. This suggests the superiority of SPS technology for preparing MAX-phases, which have the potential to be used as structural materials for high-temperature applications.

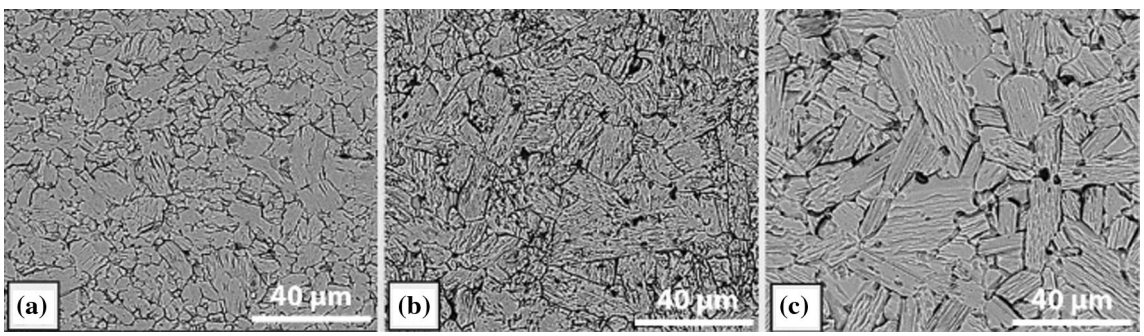

Figure 12 SEM images of samples with different grain sizes **a** fine-grained (FG) Ti_2AlC samples processed by PLS + SPS, **b** medium-grained (MG) Ti_2AlC samples processed by PLS treating FG samples for periods of 8 h and **c** coarse-grained (CG) Ti_2AlC samples processed by PLS treating FG samples for periods of 24 h, according to Ref. [225].

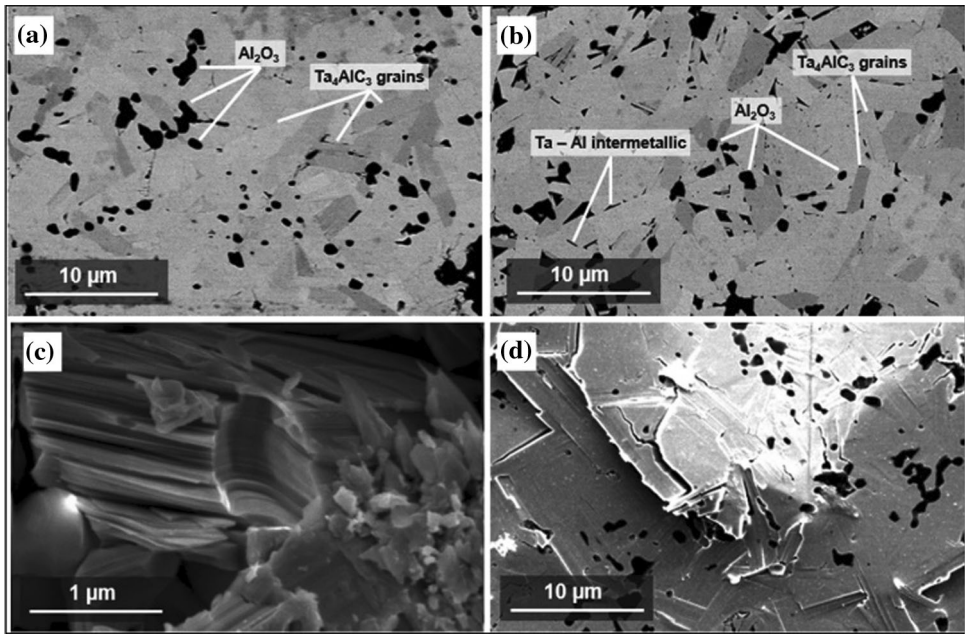

Figure 13 Backscattered electron (BSE) images of Ta_4AlC_3 produced at 1500 °C by **a** HP 20 °C min^{-1} × 30 min and **b** SPS 100 °C min^{-1} × 15 min. **c** Fracture surface showing the laminated structure of the Ta_4AlC_3 grains. **d** Typical damage near the corner of an indentation produced by a Vickers indenter, showing the dislodging of Ta_4AlC_3 MAX-phase grains [226].

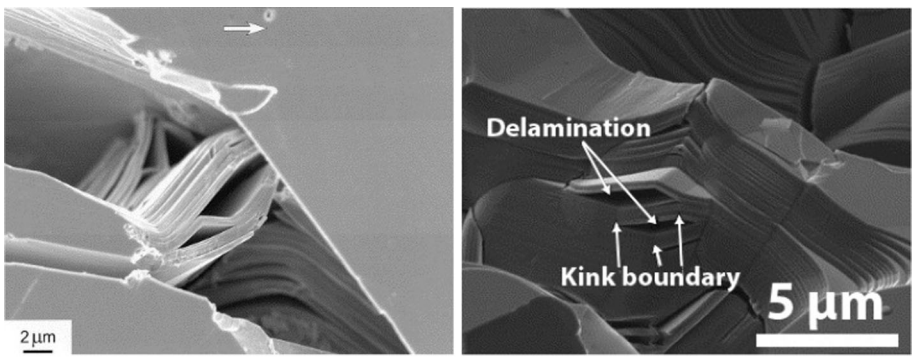

(a) (b)

Figure 14 **a** Field-emission scanning electron microscope image of a bridged crack in the coarse-grained Ti_3SiC_2 microstructure. Heavily deformed lamella bridge of the crack, and significant amounts of delamination and bending are observed. The arrow indicates the direction of crack propagation [228] and, **b** kink band formation and concomitant delaminations of a solid bridge between pores (kink boundaries and delaminations indicated with arrows) in Ti_3SiC_2 according to Ref. [229].

Besides the grain size, the effect of secondary phases on the mechanical properties of MAX-phases has also been reported. Kozak et al. [223], performing SPS on commercial powder and HP on SHSed powder respectively, prepared Ti_3SiC_2-based materials with various purity and grain sizes. The results of coupling bending tests with Acoustic Emission (AE) measurements performed on the Ti_3SiC_2-based materials with different amounts of Ti_3SiC_2 (from 52 to 72 wt%) and various mean grain sizes (from 8 to 20 μm) showed that the lower the content (wt%) of secondary phases (TiC, $TiSi_2$) is, the higher the mechanical strength and the capability to dissipate energy are, while reduction of mechanical strength and increase of dissipated energy were observed for coarse-grained material. Wan et al. [237] found that compared to monolithic $Ti_3Si_{0.95}Al_{0.05}C_2$, the SiC particle-reinforced $Ti_3Si_{0.95}Al_{0.05}C_2$–SiC composites exhibit higher elastic modulus, Vickers hardness, fracture toughness, improved wear and oxidation resistances, but demonstrate lower flexural strength. This phenomenon was attributed by the authors to the strengthening effect of SiC as the second phase on the Ti_3SiC_2-like MAX-phases. However, it is worth to remark here that for different mechanical properties, the effects of the second phase and grain size are different. For example, based on the investigation of the influence of mechanical activation process on the

mechanical properties of bulk Ti_2AlN MAX-phase obtained by reactive HP Salvo et al. [238] believed that the Ti_5Si_3 and Al_2O_3 particles dispersed into the matrix was the main factor giving rise to the enhanced Vickers hardness of mechanical activated Ti_2AlN, while the highest fractured toughness obtained by the non-mechanical activated Ti_2AlN was attributed by the authors to the large mean grain size. From this one can expect than for the MAX-phase ceramic composites, the by-product phase in which the mechanical properties of the single MAX-phase can enhance, the SPS technology is a good choice, i.e., by appropriately increasing the heating rate and reducing the sintering time one can obtain the MAX-phase ceramic composites with small grain sizes, high densification and "desired impurity (second) phases", all of which may allow improved mechanical properties of MAX-phase. As mentioned above, the SPS technology, which is good for preparing MAX-phases with small grain size and high densification as to enhance mechanical strength and inhibit the formation of kink bands, finds its limitation in improving the fracture toughness of MAX-phases. Fortunately, the second phases can make up for the lack of microstructure contribution to the fracture toughness. The mechanisms, based on which MAX-phases can be effectively toughened by the second phases particles, could be summarized as: (1) Difference in thermal expansion coefficient between the second phase and the matrix. The second phase with lower CTE compared to the matrix generates residual stresses during composite preparation (cooling process) resulting in a reduction of local stresses and strain fields at the crack tip. Therefore, crack branching, crack deflection and micro-cracking in the matrix might be favored by a residual tensile stress in the matrix [239]; (2) Clean and clear grain boundaries between reinforcements and the matrix. As shown in Fig. 15, a very close interatomic distance of close-packed planes of TiC (0.3055 nm) and TiB_2 (0.3028 nm) phases indicates the formation of coherent interface with strong binding energy [240]. Hence a transgranular fracture with increased fracture energy can be formed. Furthermore, the increase in the residual compressive stress can be also found due to the CTE mismatch, which could also lead to the increase in the crack propagation resistance; (3) The small second phase can play the role of pinning the dislocation of matrix [14]; (4) The secondary phase, which is formed as a result of the transformation process of the "original secondary phase" in the composite based on MAX-phase, generates compressive stress in the matrix [241] and toughens the matrix by multiple toughening mechanisms to a different degree, such as crack deflection and bridging [242]. Whisker and fiber can be used as excellent reinforcements for improving the fracture toughness of MAX-phase by proving ceramic matrix with large strains. However, the high reactivity between the fibers and MAX-phase matrix has narrowed the investigation works on the toughening behaviors of fiber- or whisker-reinforced MAX-phases [243]. Due to the high effectivity for toughening of MAX-phase ceramics, texture microstructure can be used instead of whisker or fiber reinforcements [224, 244–248]. As shown in Fig. 16 this can lead to grain pull-out and bridging, thereby activating the toughening mechanisms of crack deflection in MAX-phase materials [224].

The influence of sintering methods on the tribological behavior of MAX-phases can also be predicted from the work of El-Raghy et al. [249] on the effect of grain size on friction and wear behavior of Ti_3SiC_2, in which based on the sliding and abrasive wear tests it was proposed that the wear resistance increases with increasing grain size. It was believed that the increased wear resistance of coarse-grained Ti_3SiC_2 was due to a large number of possible sliding energy dissipation mechanisms such as delamination, grain deformation, microcracking, crack bridging and grain fracture compared to the fine-grained one, where only grain pull out and pre-fracture were observed. Details of the investigation results of the part of the above-selected works on mechanical properties of MAX-phases synthesized by different sintering methods are presented in Table 2.

Concluding remarks

At present, there are many methods for preparing MAX-phase materials, due to the advantages of SPS, over other sintering methods, which include enhanced densification, high heating rate, short sintering time, and low sintering temperature. SPS, as binder-less, direct, and the cost-effective process will continue to be the method of choice to develop MAX-phase that has controlled microstructures and novel properties. Furthermore, the SPS technique is highly suited toward preparing MAX-phases with small

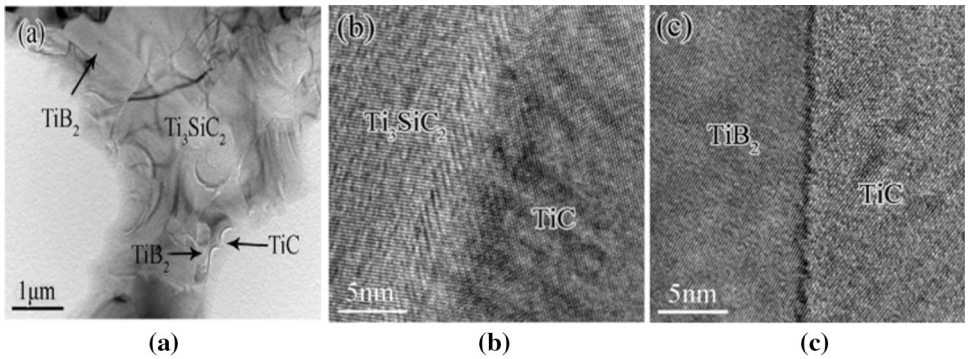

Figure 15 **a** TEM micrograph of the $(TiB_2 + TiC)/Ti_3SiC_2$ composite with 10 vol% TiB_2; **b** HRTEM image of interface structure for Ti_3SiC_2 and TiC; **c** HRTEM image of interface structure for TiB_2 and TiC [240].

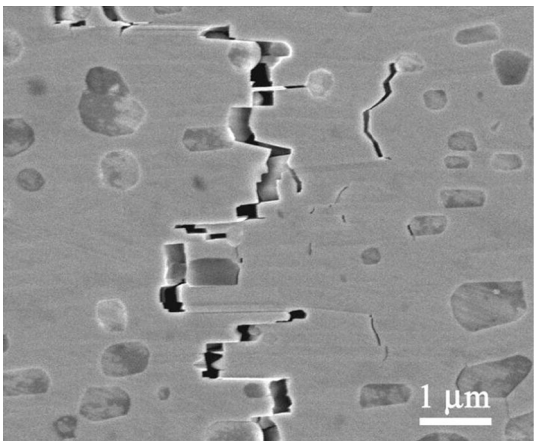

Figure 16 SEM micrographs of the in situ crack propagation of textured Nb_4AlC_3 [224].

grain size, which facilitates the increases in the mechanical strength of MAX-phases. However, it should be noted that, like all other sintering methods, the SPSed product contains certain volume of the impurity phase. This could be interpreted in three ways: (1) Stoichiometric loss always exists no matter which sintering method is applied, which leads to the formation of the undesired phases. The C-uptake from the graphite dies in the SPS process makes the selection of the molar ratios of starting materials more complicated; (2) Regardless of the sintering method, the "competition phenomenon" between the high purity and the high densification controlled by the sintering temperature and the assisting pressure always exists. Thus, the high heating rate and high assisting pressure should be applied for high densification of MAX-phases, while for synthesizing MAX-phases with high purity, smaller assisting pressure and longer holding time should be considered first; (3) The formation of the stable MAX-phases occurs only in a specific temperature interval, for which one can refer to the Ref. [250]. Below this interval, MAX-phases cannot be formed, while above this interval, MAX-phases degradation occurs. In the case of cost of preparing MAX-phases, the HP, HIP and SPS processes require precise and expensive equipment and high vacuum and protective gas (for example, argon gas), which leads to high cost of production driven by these technologies and as a result they can only be used as a conventional laboratory preparation method, not suitable for mass production of the MAX-phases. Compared with the above sintering methods, the PLS has the advantages of simple operation, high yield, and low requirements for experimental environment and technology. This is conducive to industrial production, but the problem with this method is that the PLSed products have large grain size, low densification, and inferior mechanical properties. In addition, for some MAX-phases, such as Cr_2AlC, without using ultrafine powders full densification cannot be just obtained by whether one-step PLS or two-step PLS. Furthermore, it is well admitted that small grain size allows improve most of the mechanical properties of MAX-phases, such as increase in the temperature at which graceful failure occurs, and enhancement of Vickers hardness and room temperature flexural strength, which make the SPS technology a good choice for preparing MAX-phases with excellent mechanical properties both at high temperature and room temperature. However, due to the positive effect of big grain size on the material's fracture toughness, the SPS technology should be rarely used for MAX-phases with high fracture toughness even though the grains of SPSed MAX-phases can be grown by increasing the sintering time. Thus, although MAX-phase ceramic composites exhibit excellent properties and have broad application prospects in many modern fields, to achieve large-scale industrial applications several research areas should be

Table 2 Mechanical properties of MAX-phases synthesized by different sintering methods

Sintering method	Parameters of the starting materials used for sintering	Sintering process parameters				Microstructure characteristics		
		Heating rate (°C min^{-1})	Pressure (MPa)	T (°C)	Holding time (min)	Relative density (%)	Mean grain size (μm)	Phase composition
SPS	The preceramic paper sheets with the 90 wt% Ti_3SiC_2 ceramic filler with the particle size of 1.5 μm (d50)	180	50	1200	10	Open porosity = 11.1	–	–
SPS	Vanadium powder, 250 mesh, 99.9% purity; aluminum powder, 250 mesh, 99% purity; carbon black (99.9% purity, particle size < 30 μm) powders; with composition of the V:Al:C elemental mixture 4:1.5:3 + 10 min ball milling	–	10 MPa (heating), 30 MPa (1350 °C)	1350	–	99.7 ± 0.1	–	V_4AlC_3 compound with comparatively lower amount of Al_2O_3 and VC
HP	Ti_3SiC_2 powders (average particle size 2 mm; purity > 99%) + 8 h ball milling + sieving through a 200 mesh.	–	30	1550	60	99.2	–	Ti_3SiC_2 with a small amount (less than 3vol%) of TiC
HP	Chromium (~ 32 μm, 99.95%), aluminum (~ 130 μm, 99.95%) and graphite (~ 5 μm, 99%) powders with Cr:Al:C = 2:1.1:1 + ball milling for 24 h	–	20	1400	60	–	–	Cr_2AlC (strong); Cr_7C_3 (very weak)
	Chromium with small particle size (~ 3 μm), aluminum (~ 3 μm, 99%) and graphite (~ 5 μm, 99%) powders with Cr:Al:C = 2:1.1:1 + ball milling for 24 h	–	20	1400	60	–	–	Cr_2AlC(strong); Cr_7C_3 (trace)
SPS	Chromium (~ 32 μm, 99.95%), aluminum (~ 130 μm, 99.95%) and graphite (~ 5 μm, 99%) powders with Cr:Al:C = 2:1.1:1 + ball milling for 24 h	200	50	1400	5	–	20	Cr_2AlC (strong); Cr_7C_3 (very weak)
	Chromium with small particle size (~ 3 μm), aluminum (~ 3 μm, 99%) and graphite (~ 5 μm, 99%) powders with Cr:Al:C = 2:1.1:1 + ball milling for 24 h	200	50	1400	5	–	5	Cr_2AlC(strong); Cr_7C_3 (trace)

Table 2 continued

Sintering method	Parameters of the starting materials used for sintering	Sintering process parameters				Microstructure characteristics		
		Heating rate (°C min^{-1})	Pressure (MPa)	T (°C)	Holding time (min)	Relative density (%)	Mean grain size (μm)	Phase composition
HP	Milled Ta_2H (particle size < 10 μm, purity 99.95%) Al (particle size < 5 μm, > 99% purity) and C (particle size < 5 μm, > 99% purity) with Ta:Al:C ratio = 4:1.25:2.6	20	30	1500	30	93.6	Length = 6 ± 1 μm; width = 1.7 ± 1 μm	α-Ta_4AlC_3 (99 wt%); Ta_2AlC (1 wt%) with a low concentration of Al_2O_3
HP	AlN and Ti powders (99.5% purity) with particle size lower than 44 μm in the Ti:AlN = 2:1 molar ratio	3 °C/min from room temperature (RT) to 100 °C and 10 °C/min from 100 to 1200 °C.	30	1200	120	95.6 ± 0.2	11.2 ± 2.3	Ti_2AlN (91.5 wt%); TiN (4.6 wt%); TiAl (3.9 wt%)
mechanical activation process + HP	AlN and Ti powders (99.5% purity) with particle size lower than 44 μm in the Ti:AlN = 2:1 molar ratio + mechanical activation by a milling process for 10 h	3 °C/min from room temperature (RT) to 100 °C and 10 °C/min from 100 to 1200 °C.	30	1200	120	97.7 ± 0.5	6.9 ± 2.1	Ti_2AlN (74.3 wt%); TiN (15.0 wt%); Ti_5Si_3 (4.9 wt%); Al_2O_3 (5.8 wt%)

Sintering method	Parameters of the starting materials used for sintering	Mechanical properties				Ref.
		Vickers hardness (GPa)	Young's modulus (GPa)	Flexural (bending) strength (MPa)	Fracture toughness (MPa $m^{1/2}$)	
SPS	The preceramic paper sheets with the 90 wt% Ti_3SiC_2 ceramic filler with the particle size of 1.5 μm (d50)	–	200	300	–	[110]
SPS	Vanadium powder, 250 mesh, 99.9% purity; aluminum powder, 250 mesh, 99% purity; carbon black (99.9% purity, particle size < 30 μm) powders; with composition of the V:Al:C elemental mixture 4:1.5:3 + 10 min ball milling	6.74 ± 0.12	–	389 ± 19	–	[150]
HP	Ti_3SiC_2 powders (average particle size 2 mm; purity > 99%) + 8 h ball milling + sieving through a 200 mesh.	–	378.4	452 ± 30	6.23 ± 0.22	[153]

Table 2 continued

Sintering method	Parameters of the starting materials used for sintering	Mechanical properties				Ref.
		Vickers hardness (GPa)	Young's modulus (GPa)	Flexural (bending) strength (MPa)	Fracture toughness (MPa $m^{1/2}$)	
HP	Chromium (~ 32 μm, 99.95%), aluminum (~ 130 μm, 99.95%) and graphite (~ 5 μm, 99%) powders with Cr:Al:C = 2:1.1:1 + ball milling for 24 h	3.5	–	–	–	[222]
	Chromium with small particle size (~ 3 μm), aluminum (~ 3 μm, 99%) and graphite (~ 5 μm, 99%) powders with Cr:Al:C = 2:1.1:1 + ball milling for 24 h	4.5	–	–	–	[222]
SPS	Chromium (~ 32 μm, 99.95%), aluminum (~ 130 μm, 99.95%) and graphite (~ 5 μm, 99%) powders with Cr:Al:C = 2:1.1:1 + ball milling for 24 h	3.9	–	–	–	[222]
	Chromium with small particle size (~ 3 μm), aluminum (~ 3 μm, 99%) and graphite (~ 5 μm, 99%) powders with Cr:Al:C = 2:1.1:1 + ball milling for 24 h	5.6	–	–	–	[222]
HP	Milled Ta_2H (particle size < 10 μm, purity 99.95%) Al (particle size < 5 μm, > 99% purity) and C (particle size < 5 μm, > 99% purity) with Ta:Al:C ratio = 4:1.25:2.6	6.1 ± 0.4	248 ± 27	407 ± 50	5.0 ± 0.6	[226]
HP	AlN and Ti powders (99.5% purity) with particle size lower than 44 μm in the Ti:AlN = 2:1 molar ratio	4.3 ± 0.4	–	–	4.8 ± 0.7	[238]
mechanical activation process + HP	AlN and Ti powders (99.5% purity) with particle size lower than 44 μm in the Ti:AlN = 2:1 molar ratio + mechanical activation by a milling process for 10 h	5.9 ± 0.7	–	–	3.9 ± 0.5	[238]

developed: (1) Using theoretical calculations for obtaining the thermodynamic stability of MAX-phases depending on the temperature, thereby guiding the selection of sintering methods and adjustment of the sintering temperature in order to experimentally synthesize and sinter new MAX-phases; (2) Investigation of the influence of sintering parameters applied in various sintering processes, such as the molar ratios of starting materials, heating rate, holding time, and the assisting pressure, on the purity, the density and the microstructure of MAX-phases, the impact of which was found to be especially severe in the mechanical properties of MAX-phases; (3) Reduction of the production costs and simplification of the synthesis process while improving the purity of synthesized MAX-phases.

New approaches based on both new starting components and additive technologies can be used to produce new materials based on the MAX-phases [251–253]. Currently, new technologies to obtain laminated [254] or preceramic paper-derived structures [111] are being developed, and their application open the potential for manufacturing of gradient (in relation to composition and porosity) MAX-phase materials with complex shape. Gradient MAX-phase materials can have superior mechanical properties due to the layered structure providing crack resistance, as well as enhanced high-temperature resistance that can be achieved by designing of multi-level structure with gradually changing thermal expansion coefficient. At the same time, the mechanical properties of MAX-phase-based materials can be increased by fiber reinforcement, which has been shown in recent works [255–261] and review on toughening mechanisms in MAX-phase ceramics [243]. SPS can be expected to be beneficial method due to that in the traditional sintering process, the required high sintering temperature and long sintering time lead to the degradation of the fibers, and even to the chemical reaction between the fiber and the matrix. In this context, due to the fast sintering process, the SPS method can be used to obtain fiber-reinforced MAX-phase ceramics without damaging the reinforcing fibers [262].

Acknowledgements

The work was supported by the Russian Science Foundation (Grant No. 19-19-00192). The authors also acknowledge Tomsk Polytechnic University Competitiveness Enhancement Program.

Compliance with ethical standards

Conflict of interest The authors declare no conflict of interest.

References

[1] Xie Y-p, Bao J-f (2017) Process of MAX phase materials. J Jilin Inst Chem Technol 34:81–85. https://doi.org/10.16039/j.cnki.cn22-1249.2017.11.018 **(in Chinese)**

[2] Barsoum MW (2000) The M(N + 1)AX(N) phases: a new class of solids; thermodynamically stable nanolaminates. Prog Solid State Chem 28:201–281. https://doi.org/10.1016/s0079-6786(00)00006-6

[3] Wang ZY, Li WT, Wang CC, Wu HC, Ke PL, Wang AY (2020) Transforming the amorphous Ti–Al–C coatings to high-purity Ti_2AlC MAX phase coatings by prolonged annealing at 550 °C. Mater Lett 261:127160. https://doi.org/10.1016/j.matlet.2019.127160

[4] Tang CC, Steinbruck M, Klimenkov M, Jantsch U, Seifert HJ, Ulrich S, Stuber M (2020) Textured growth of polycrystalline MAX phase carbide coatings via thermal annealing of M/C/Al multilayers. J Vac Sci Technol A 38:013401. https://doi.org/10.1116/1.5131544

[5] Zhang S, Shi L, Mercier F, Chaix-Pluchery O, Chaussende D, Gelard I, Hackens B, Ouisse T (2017) Conversion of MAX phase single crystals in highly porous carbides by high temperature chlorination. Ceram Int 43:8246–8254. https://doi.org/10.1016/j.ceramint.2017.03.153

[6] Hu CF, Zhang HB, Li FZ, Huang Q, Bao YW (2013) New phases' discovery in MAX family. Int J Refract Met Hard Mat 36:300–312. https://doi.org/10.1016/j.ijrmhm.2012.10.011

[7] Haemers J, Gusmao R, Sofer Z (2020) Synthesis protocols of the most common layered carbide and nitride MAX phases. Small Methods 4:1900780. https://doi.org/10.1002/smtd.201900780

[8] Tao QZ, Lu J, Dahlqvist M, Mockute A, Calder S, Petruhins A, Meshkian R, Rivin O et al (2019) atomically layered and ordered rare-earth i-MAX phases: a new class of magnetic quaternary compounds. Chem Mater 31:2476–2485. https://doi.org/10.1021/acs.chemmater.8b05298

[9] Fashandi H, Dahlqvist M, Lu J, Palisaitis J, Simak SI, Abrikosov IA, Rosen J, Hultman L et al (2017) Synthesis of Ti_3AuC_2, $Ti_3Au_2C_2$ and Ti_3IrC_2 by noble metal substitution reaction in Ti_3SiC_2 for high-temperature-stable Ohmic

contacts to SiC. Nat Mater 16:814–818. https://doi.org/10.1038/nmat4896

[10] Li M, Lu J, Luo K, Li YB, Chang KK, Chen K, Zhou J, Rosen J et al (2019) Element replacement approach by reaction with lewis acidic molten salts to synthesize nanolaminated MAX phases and MXenes. J Am Chem Soc 141:4730–4737. https://doi.org/10.1021/jacs.9b00574

[11] Li YB, Li M, Lu J, Ma BK, Wang ZP, Cheong LZ, Luo K, Zha XH et al (2019) Single-atom-thick active layers realized in nanolaminated Ti-3(AlxCu1-x)C-2 and its artificial enzyme behavior. ACS Nano 13:9198–9205. https://doi.org/10.1021/acsnano.9b03530

[12] Wang JJ, Ye TN, Gong YT, Wu JZ, Miao NX, Tada T, Hosono H (2019) Discovery of hexagonal ternary phase Ti_2InB_2 and its evolution to layered boride TiB. Nat Commun 10:2284. https://doi.org/10.1038/s41467-019-10297-8

[13] Chakraborty P, Chakrabarty A, Dutta A, Saha-Dasgupta T (2018) Soft MAX phases with boron substitution: a computational prediction. Phys Rev Mater 2:103605. https://doi.org/10.1103/PhysRevMaterials.2.103605

[14] Zheng L, Zhou Y, Feng Z (2013) Preparation, structural featrures, properties and prospective of MAX hases. Aerosp Mater Technol 43:1–23. https://doi.org/10.3969/j.issn.1007-2330.2013.06.001 **(in Chinese)**

[15] Liu Y-L, Zhu D-G, Hu C-F (2017) Review of MAX phases and its coating fabricated by spraying. Adv Ceram 38:21–28. https://doi.org/10.16253/j.cnki.37-1226/tq.2016.09.003 **(in Chinese)**

[16] Li J-H, Zhang C, Wang X-H (2017) Progress in machinable and electrically conductive laminated ternary ceramics (MAX Phases). Adv Ceram 38:3–20. https://doi.org/10.16253/j.cnki.37-1226/tq.2016.09.007 **(in Chinese)**

[17] Magnuson M, Mattesini M (2017) Chemical bonding and electronic-structure in MAX phases as viewed by X-ray spectroscopy and density functional theory. Thin Solid Films 621:108–130. https://doi.org/10.1016/j.tsf.2016.11.005

[18] Gonzalez-Julian J, Onrubia S, Bram M, Guillon O (2016) Effect of sintering method on the microstructure of pure Cr_2AlC MAX phase ceramics. J Ceram Soc Jpn 124:415–420. https://doi.org/10.2109/jcersj2.15263

[19] Zhang H, Hu T, Wang XH, Zhou YC (2020) Structural defects in MAX phases and their derivative MXenes: a look forward. J Mater Sci Technol 38:205–220. https://doi.org/10.1016/j.jmst.2019.03.049

[20] Tallman DJ, Anasori B, Barsoum MW (2013) A critical review of the oxidation of Ti_2AlC, Ti_3AlC_2 and Cr_2AlC in Air. Mater Res Lett 1:115–125. https://doi.org/10.1080/21663831.2013.806364

[21] Gu J, Jiang X, Guo W, Li P, Liu C, Chen F (2016) Research progress of layered ternary ceramic of Nb_4AlC_3. Jiangsu Ceram 49(6–8):19. https://doi.org/10.3969/j.issn.1006-7337.2016.05.003 **(in Chinese)**

[22] Tallman DJ, He LF, Gan J, Caspi EN, Hoffman EN, Barsoum MW (2017) Effects of neutron irradiation of Ti_3SiC_2 and Ti_3AlC_2 in the 121–1085 °C temperature range. J Nucl Mater 484:120–134. https://doi.org/10.1016/j.jnucmat.2016.11.016

[23] Ward J, Bowden D, Prestat E, Holdsworth S, Stewart D, Barsoum MW, Preuss M, Frankel P (2018) Corrosion performance of Ti_3SiC_2, Ti_3AlC_2, Ti_2AlC and Cr_2AlC MAX phases in simulated primary water conditions. Corrosion Sci 139:444–453. https://doi.org/10.1016/j.corsci.2018.04.034

[24] Smialek JL, Nesbitt JA, Gabb TP, Garg A, Miller RA (2018) Hot corrosion and low cycle fatigue of a Cr_2AlC-coated superalloy. Mater Sci Eng A Struct Mater Prop Microstruct Process 711:119–129. https://doi.org/10.1016/j.msea.2017.10.098

[25] Mahmoudi Z, Tabaian SH, Rezaie HR, Mahboubi F, Ghazali MJ (2020) Synthesis of Ti_2AlC & Ti_3AlC_2 MAX phases by Arc-PVD using Ti-Al target in C_2H_2/Ar gas mixture and subsequent annealing. Ceram Int 46:4968–4975. https://doi.org/10.1016/j.ceramint.2019.10.235

[26] Berger O (2020) The correlation between structure, multifunctional properties and applications of PVD MAX phase coatings. Part II. Texture and high-temperature properties. Surf Eng 36:268–302. https://doi.org/10.1080/02670844.2019.1611076

[27] Zhang FY, Yan S, Li C, Ding Y, He JN, Yin FX (2019) Synthesis and characterization of MAX phase Cr_2AlC based composite coatings by plasma spraying and post annealing. J Eur Ceram Soc 39:5132–5139. https://doi.org/10.1016/j.jeurceramsoc.2019.08.039

[28] Van Loo K, Lapauw T, Ozalp N, Strom E, Lambrinou K, Vleugels J (2019) Compatibility of SiC-and MAX phase-based ceramics with a KNO_3–$NaNO_3$ molten solar salt. Sol Energy Mater Sol Cells 195:228–240. https://doi.org/10.1016/j.solmat.2019.03.007

[29] Prikhna TO, Podhurs'ka VY, Ostash OP, Vasyliv BD, Sverdun VB, Karpets MV, Serbenyuk TB (2019) Influence of the technology of production of composites based on the max phases of titanium on the process of wear in contact with copper. Part 1. Two-stage technology. Mater Sci 54:589–595. https://doi.org/10.1007/s11003-019-00222-1

[30] Liu Y, Qu YP, Xin JH, Wang ZH, Fan GH, Xie PT, Sun K (2019) Weakly radio-frequency negative permittivity of poly(vinylidene fluoride)/Ti_3SiC_2 MAX phase

metacomposites. J Inorg Organomet Polym Mater 29:248–257. https://doi.org/10.1007/s10904-018-0983-8

[31] Lu JL, Abbas N, Tang JN, Tang J, Zhu GM (2019) Synthesis and characterization of conductive ceramic MAX-phase coatings for metal bipolar plates in simulated PEMFC environments. Corrosion Sci 158:108106. https://doi.org/10.1016/j.corsci.2019.108106

[32] Derradji M, Henniche A, Wang J, Dayo AQ, Ouyang JH, Liu WB, Medjahed A (2018) High performance nanocomposites from Ti_3SiC_2 MAX phase and phthalonitrile resin. Polym Compos 39:3705–3711. https://doi.org/10.1002/pc.24401

[33] Su RR, Zhang HL, O'Connor DJ, Shi LQ, Meng XP, Zhang HB (2016) Deposition and characterization of Ti_2AlC MAX phase and Ti_3AlC thin films by magnetron sputtering. Mater Lett 179:194–197. https://doi.org/10.1016/j.matlet.2016.05.086

[34] Hettinger JD, Lofland SE, Finkel P, Meehan T, Palma J, Harrell K, Gupta S, Ganguly A et al (2005) Electrical transport, thermal transport, and elastic properties of M_2AlC (M = Ti, Cr, Nb, and V). Phys Rev B 72:115120. https://doi.org/10.1103/PhysRevB.72.115120

[35] Galyshev S, Bazhin P, Stolin A, Musin F, Astanin V (2017) Heat treatment of composite based on MAX-phases of the Ti–Al–C system. MATEC Web Conf 129:02011. https://doi.org/10.1051/matecconf/201712902011

[36] Zhan Z, Liu Y, Wang W (2012) Review of layered ternary compound MAX phases. J Yanshan Univ 36:189–195. https://doi.org/10.3969/j.issn.1007-791X.2012.03.001 **(in Chinese)**

[37] Sokol M, Natu V, Kota S, Barsoum MW (2019) On the chemical diversity of the MAX phases. Trends Chem 1:210–223. https://doi.org/10.1016/j.trechm.2019.02.016

[38] Bai Y, Liu J, Jin Y (2017) Research progress of layered Cr_2AlC ternary ceramic. China Ceram Ind 24:22–29. https://doi.org/10.13958/j.cnki.ztcg.2017.05.004 **(in Chinese)**

[39] Lei Y, Liu J, Jin Y, An X, Chen Y (2013) Current research status and development of layered ternary ceramic material Cr_2AlC. J Xihua Univ Nat Sci Ed 32:77–81. https://doi.org/10.3969/j.issn.1673-159x.2013.01.015 **(in Chinese)**

[40] Ren Y, Sun N, Guan C, Sun R, Chu X, Liu D, Wei Z, Lou L et al (2016) Research progress of layered ternary ceramic material of Ti_2SC. China Ceram 52:1–6. https://doi.org/10.16521/j.cnki.issn.1001-9642.2016.12.001 **(in Chinese)**

[41] Lian R, Li Y, Bai P, Jia F (2016) Research progress of ternary compound Ti_3SiC_2. Foundy Technol 37:209–211. https://doi.org/10.16410/j.issn1000-8365.2016.02.003 **(in Chinese)**

[42] An N, Liu Y (2014) Research progress of layered ceramic Ti_3SiC_2. Chin J Pract Stomatol 7:125–128 **(in Chinese)**

[43] Lu L, Yin H, Yuan H (2012) Research progress of the layered Ti_3SiC_2 ceramics. J Ceram 33:226–229. https://doi.org/10.3969/j.issn.1000-2278.2012.02.023 **(in Chinese)**

[44] Qian Y, Zhu J, Zhu C (2012) Research progress on the layered ternary ceramic Ti_3AlC_2. Mater Rev 26:150–154. https://doi.org/10.3969/j.issn.1005-023x.2012.23.033 **(in Chinese)**

[45] Li M, Huang Q (2020) Recent progress and prospects of ternary layered carbides/nitrides MAX phases and their derived two-dimensional nanolaminates MXenes. J Inorg Mater 35:1–7. https://doi.org/10.15541/jim20190560

[46] Biesuz M, Sglavo VM (2019) Flash sintering of ceramics. J Eur Ceram Soc 39:115–143. https://doi.org/10.1016/j.jeurceramsoc.2018.08.048

[47] Chaim R, Chevallier G, Weibel A, Estournes C (2018) Grain growth during spark plasma and flash sintering of ceramic nanoparticles: a review. J Mater Sci 53:3087–3105. https://doi.org/10.1007/s10853-017-1761-7

[48] Rajkumar Y, Rahul B, Akash PA, Panigrahi B (2017) Nonisothermal sintering of Cr_2AlC powder. Int J Appl Ceram Technol 14:63–67. https://doi.org/10.1111/ijac.12617

[49] Rajkumar Y, Panigrahi BB (2016) Sintering mechanisms of ultrafine Cr_2AlC MAX phase powder. Mater Today Commun 8:46–52. https://doi.org/10.1016/j.mtcomm.2016.05.002

[50] Su ZL, Zeng S, Zhou J, Sun ZM (2014) Synthesis and characterization of Cr_2AlC with nanolaminated particles. Chin Sci Bull 59:3266–3270. https://doi.org/10.1007/s11434-014-0315-5

[51] Mane RB, Haribabu A, Panigrahi BB (2018) Synthesis and sintering of Ti_3GeC_2 MAX phase powders. Ceram Int 44:890–893. https://doi.org/10.1016/j.ceramint.2017.10.017

[52] Guillon O, Gonzalez-Julian J, Dargatz B, Kessel T, Schierning G, Rathel J, Herrmann M (2014) Field-assisted sintering technology/spark plasma sintering: mechanisms, materials, and technology developments. Adv Eng Mater 16:830–849. https://doi.org/10.1002/adem.201300409

[53] Shamsipoor A, Farvizi M, Razavi M, Keyvani A (2020) Influences of processing parameters on the microstructure and wear performance of Cr_2AlC MAX phase prepared by spark plasma sintering method. J Alloys Compd 815:152345. https://doi.org/10.1016/j.jallcom.2019.152345

[54] Li SB, Xiao LO, Song GM, Wu XM, Sloof WG, van der Zwaag S (2013) Oxidation and crack healing behavior of a fine-grained Cr_2AlC ceramic. J Am Ceram Soc 96:892–899. https://doi.org/10.1111/jace.12170

[55] Tian WB, Wang PL, Kan YM, Zhang GJ, Li YX, Yan DS (2007) Phase formation sequence of Cr_2AlC ceramics

starting from Cr–Al–C powders. Mater Sci Eng A Struct Mater Prop Microstruct Process 443:229–234. https://doi.org/10.1016/j.msea.2006.08.064

[56] Li SB, Zhai HX, Zhou Y, Zhang ZL (2005) Synthesis of Ti_3SiC_2 powders by mechanically activated sintering of elemental powders of Ti, Si and C. Mater Sci Eng A Struct Mater Prop Microstruct Process 407:315–321. https://doi.org/10.1016/j.msea.2005.07.043

[57] Yan M, Chen Y-l, Mei B-c, Zhu J-q (2008) Synthesis of high-purity Ti_2AlN ceramic by hot pressing. Trans Nonferrous Met Soc China 18:82–85. https://doi.org/10.1016/S1003-6326(08)60015-1

[58] Wang P, Mei B-c, Hong X-l, Zhou W-b (2007) Synthesis of Ti_2AlC by hot pressing and its mechanical and electrical properties. Trans Nonferrous Met Soc China 17:1001–1004. https://doi.org/10.1016/S1003-6326(07)60215-5

[59] Shang W (2010) Development and application of hot isostatic pressing (HIP) technology and equipments. Nonferr Met Eng Res 31:18–21. https://doi.org/10.3969/j.issn.1004-4345.2010.01.007 **(in Chinese)**

[60] Zhu Z, Tian X (2010) Application and development of isostatic pressing technology. Adv Ceram 31:17–24. https://doi.org/10.3969/j.issn.1005-1198.2010.01.004 **(in Chinese)**

[61] Liu H, He R, Zhou W, Wang T (2010) Development and application of hot isostatic pressing technology. Adv Mater Ind. https://doi.org/10.3969/j.issn.1008-892x.2010.11.003 **(in Chinese)**

[62] Tunca B, Lapauw T, Delville R, Neuville DR, Hennet L, Thiaudiere D, Ouisse T, Hadermann J et al (2019) Synthesis and characterization of double solid solution (Zr, Ti)(2)(Al, Sn)C MAX phase ceramics. Inorg Chem 58:6669–6683. https://doi.org/10.1021/acs.inorgchem.9b00065

[63] Zhan Z (2005) Application and development of hot isostatic pressing technology and apparatus. China Tungsten Ind 20:44–47. https://doi.org/10.3969/j.issn.1009-0622.2005.01.012 **(in Chinese)**

[64] Suijiazhuang (2018) Advantages of hot pressing sintering. https://wenku.baidu.com/view/d71f70ccf6ec4afe04a1b0717fd5360cbb1a8d0d.html. Accessed 28 Oct 2018 **(in Chinese)**

[65] Xiaofuzi (2018) Chapter 7 Hot Press Sintering. https://wenku.baidu.com/view/aab032446fdb6f1aff00bed5b9f3f90f76c64d89.html?fr=search. Accessed 12 Oct 2018 **(in Chinese)**

[66] Nongminbaibaiwenku (2018) Hot Press Sintering (in Chinese). https://wenku.baidu.com/view/047b86c0970590c69ec3d5bbfd0a79563c1ed482.html. Accessed 05 October 2018

[67] Lopacinski M, Puszynski J, Lis J (2001) Synthesis of ternary titanium aluminum carbides using self-propagating high-temperature synthesis technique. J Am Ceram Soc 84:3051–3053. https://doi.org/10.1111/j.1151-2916.2001.tb01138.x

[68] Zhu CC, Zhu J, Wu H, Lin H (2015) Synthesis of Ti_3AlC_2 by SHS and thermodynamic calculation based on first principles. Rare Met 34:107–110. https://doi.org/10.1007/s12598-013-0174-2

[69] Vadchenko SG, Sytschev AE, Kovalev DY, Shchukin AS, Konovalikhin SV (2015) Self-propagating high-temperature synthesis in the Ti–Si–C system: features of product patterning. Nanotechnol Russ 10:67–74. https://doi.org/10.1134/s1995078015010206

[70] Luo L, Zhang Y, Zan X, Liu J, Zhu X, Wu Y (2018) Status and development of self-propagating high-temperature synthesis of high melting point powders. Chin J Rare Met 42:1210–1220. https://doi.org/10.13373/j.cnki.cjrm.XY17110004 **(in Chinese)**

[71] Novak P, Skolakova A, Pignol D, Prusa F, Salvetr P, Kubatik TF, Perriere L, Karlik M (2016) Finding the energy source for self-propagating high-temperature synthesis production of NiTi shape memory alloy. Mater Chem Phys 181:295–300. https://doi.org/10.1016/j.matchemphys.2016.06.062

[72] Zhou Y, Zhang ZT, Jin X, Ye GT, Liu CY (2016) Fabrication and composition investigation of $WSi_2/MoSi_2$ composite powders obtained by a self-propagating high-temperature synthesis method. Arab J Sci Eng 41:2583–2587. https://doi.org/10.1007/s13369-016-2072-z

[73] Dine S, Kentheswaran V, Vrel D, Couzinie JP, Dirras G (2017) Synthesis of nanometric MoNbW alloy using self-propagating high-temperature synthesis. Adv Powder Technol 28:1739–1744. https://doi.org/10.1016/j.apt.2017.04.011

[74] Liu X, Yang M (2010) The research on technology of self-sustaining high-temperature synthesis matal-matrix ceramics compsosite. Mod Mach. https://doi.org/10.3969/j.issn.1002-6886.2010.05.033 **(in Chinese)**

[75] Gorshkov VA, Miloserdov PA, Sachkova NV (2020) High-temperature synthesis of cast materials based on the MAX phase Cr_2AlC using $CaCrO_4 + Al + C$ mixtures. Inorg Mater 56:321–327. https://doi.org/10.1134/s0020168520030048

[76] Gorshkov VA, Miloserdov PA, Luginina MA, Sachkova NV, Belikova AF (2017) High-temperature synthesis of a cast material with a maximum content of the MAX phase Cr_2AlC. Inorg Mater 53:271–277. https://doi.org/10.1134/s0020168517030062

[77] Tomoshige R, Ishida K, Inokawa H (2019) Effect of added molybdenum on material properties of Zr_2SC MAX phase produced by self-propagating high temperature synthesis. Mater Res Proc 13:79–84. https://doi.org/10.21741/9781644900338-14

[78] Yeh CL, Chiang CH (2017) Combustion synthesis of MAX phase solid solution Ti-3(Al, Sn)C-2. Nano Hybrids Compos 16:73–76. https://doi.org/10.4028/www.scientific.net/NHC.16.73

[79] Kovalev DY, Luginina MA, Vadchenko SG, Konovalikhin SV, Sychev AE, Shchukin AS (2017) Synthesis of a new MAX phase in the Ti–Zr–Al–C system. Mendeleev Commun 27:59–60. https://doi.org/10.1016/j.mencom.2017.01.018

[80] Zuo B-l, Liu P-j, Zhang W-h, Yan Q-l (2018) Recent progress on the functional materials synthesized by high temperature self-propagating reactions. Chin J Energ Mater 26:537–544. https://doi.org/10.11943/j.issn.1006-9941.2018.06.012 **(in Chinese)**

[81] Renshen (2019) Self-propagating high-temperature synthesis. https://wenku.baidu.com/view/ddcefa4b7e192279168884868762caaedc33ba39.html?fr=search. Accessed 9 May 2019 **(in Chinese)**

[82] Potanin AY, Loginov PA, Levashov EA, Pogozhev YS, Patsera EI, Kochetov NA (2015) Effect of mechanical activation on Ti_3AlC_2 max phase formation under self-propagating high-temperature synthesis. Eurasian Chem Technol J 17:233–242. https://doi.org/10.18321/ectj249

[83] Cuskelly D, Richards E, Kisi E (2016) MAX phase–alumina composites via elemental and exchange reactions in the Tin + 1ACn systems (A = Al, Si, Ga, Ge, In and Sn). J Solid State Chem 237:48–56. https://doi.org/10.1016/j.jssc.2016.01.014

[84] Azarniya A, Azarniya A, Safavi MS, Ahmadipour MF, Seraji ME, Sovizi S, Saqaei M, Yamanoglu R et al (2020) Physicomechanical properties of porous materials by spark plasma sintering. Crit Rev Solid State Mater Sci 45:22–65. https://doi.org/10.1080/10408436.2018.1532393

[85] Munir ZA, Quach DV, Ohyanagi M (2011) Electric current activation of sintering: a review of the pulsed electric current sintering process. J Am Ceram Soc 94:1–19. https://doi.org/10.1111/j.1551-2916.2010.04210.x

[86] Garay JE (2010) Current-activated, pressure-assisted densification of materials. Ann Rev Mater Res 40:445–468. https://doi.org/10.1146/annurev-matsci-070909-104433

[87] Wang LJ, Zhang JF, Jiang W (2013) Recent development in reactive synthesis of nanostructured bulk materials by spark plasma sintering. Int J Refract Met Hard Mater 39:103–112. https://doi.org/10.1016/j.ijrmhm.2013.01.017

[88] Dudina DV, Bokhonov BB, Olevsky EA (2019) Fabrication of porous materials by spark plasma sintering: a review. Materials 12(28):541. https://doi.org/10.3390/ma12030541

[89] Dudina DV, Mukherjee AK (2013) Reactive spark plasma sintering: successes and challenges of nanomaterial synthesis. J Nanomater 2013:625218. https://doi.org/10.1155/2013/625218

[90] Salamon D, Maca K, Shen ZJ (2012) Rapid sintering of crack-free zirconia ceramics by pressure-less spark plasma sintering. Scr Mater 66:899–902. https://doi.org/10.1016/j.scriptamat.2012.02.013

[91] Salamon D, Kalousek R, Maca K, Shen ZJ (2015) Rapid grain growth in 3Y-TZP nanoceramics by pressure-assisted and pressure-less SPS. J Am Ceram Soc 98:3706–3712. https://doi.org/10.1111/jace.13837

[92] Hulbert DM, Anders A, Andersson J, Lavernia EJ, Mukherjee AK (2009) A discussion on the absence of plasma in spark plasma sintering. Scr Mater 60:835–838. https://doi.org/10.1016/j.scriptamat.2008.12.059

[93] Guyot P, Rat V, Coudert JF, Jay F, Maitre A, Pradeilles N (2012) Does the Branly effect occur in spark plasma sintering? J Phys D Appl Phys 45:092001. https://doi.org/10.1088/0022-3727/45/9/092001

[94] Chaim R (2008) Densification mechanisms in spark plasma sintering of nanocrystalline ceramics (vol 443, pg 25, 2007). Mater Sci Eng A Struct Mater Prop Microstruct Process 486:696. https://doi.org/10.1016/j.msea.2008.02.031

[95] Chaim R (2016) On densification mechanisms of ceramic particles during spark plasma sintering. Scr Mater 115:84–86. https://doi.org/10.1016/j.scriptamat.2016.01.010

[96] Orru R, Cao G (2013) Comparison of reactive and non-reactive spark plasma sintering routes for the fabrication of monolithic and composite ultra high temperature ceramics (UHTC) materials. Materials 6:1566–1583. https://doi.org/10.3390/ma6051566

[97] Saheb N, Iqbal Z, Khalil A, Hakeem AS, Al Aqeeli N, Laoui T, Al-Qutub A, Kirchner R (2012) Spark plasma sintering of metals and metal matrix nanocomposites: a review. J Nanomater 13:983470. https://doi.org/10.1155/2012/983470

[98] Saheb N, Hayat U, Hassan SF (2019) Recent advances and future prospects in spark plasma sintered alumina hybrid nanocomposites. Nanomaterials 9:1607. https://doi.org/10.3390/nano9111607

[99] Marder R, Estournes C, Chevallier G, Chaim R (2014) Plasma in spark plasma sintering of ceramic particle compacts. Scr Mater 82:57–60. https://doi.org/10.1016/j.scriptamat.2014.03.023

[100] Wang Q, Zhang Y, Guo X, Song K (2014) The latest development and research progress of spark plasma sintering process. Rare Met Cem Carbides 42:44–47 **(in Chinese)**

[101] Dong P, Wang Z, Wang WX, Chen SP, Zhou J (2016) Understanding the spark plasma sintering from the view of materials joining. Scr Mater 123:118–121. https://doi.org/10.1016/j.scriptamat.2016.06.014

[102] Zhang ZH, Liu ZF, Lu JF, Shen XB, Wang FC, Wang YD (2014) The sintering mechanism in spark plasma sintering—proof of the occurrence of spark discharge. Scr Mater 81:56–59. https://doi.org/10.1016/j.scriptamat.2014.03.011

[103] Hitchcock D, Livingston R, Liebenberg D (2015) Improved understanding of the spark plasma sintering process. J Appl Phys 117:174505. https://doi.org/10.1063/1.4919814

[104] Wang S, Xie M, Zhang J, Yang Y, Liu M, Chen Y, Wang S (2012) Development of spark plasma sintering technology. Precious Met 33:73–77. https://doi.org/10.3969/j.issn.1004-0676.2012.03.012 **(in Chinese)**

[105] Yan Q (2016) Research progress of spark plasma sintering. Sci Technol Innov Her 13:36–37. https://doi.org/10.16660/j.cnki.1674-098x.2016.31.036 **(in Chinese)**

[106] Meng Y, Qiang W, Jia C (2014) Status quo of spark plasma sintering in Japan. Powder Metall Technol 32:296–305 **(in Chinese)**

[107] Angerer P, Yu LG, Khor KA, Krumpel G (2004) Spark-plasma-sintering (SPS) of nanostructured and submicron titanium oxide powders. Mater Sci Eng A Struct Mater Prop Microstruct Process 381:16–19. https://doi.org/10.1016/j.msea.2004.02.009

[108] Wang JM, Gao L (2005) Photoluminescence properties of nanocrystalline ZnO ceramics prepared by pressureless sintering and spark plasma sintering. J Am Ceram Soc 88:1637–1639. https://doi.org/10.1111/j.1551-2916.2005.00259.x

[109] Shao C, Zhang G, Cheng P, Qin G (2011) Research progress of processable ternary layered conductive ceramic Ti_3SiC_2. Chin Mater Sci Technol Equip 4:15–18 **(in Chinese)**

[110] Kashkarov EB, Syrtanov MS, Sedanova EP, Ivashutenko AS, Lider AM, Travitzky N (2020) Fabrication of paper-derived Ti_3SiC_2-based materials by spark plasma sintering. Adv Eng Mater 22:2000136. https://doi.org/10.1002/adem.202000136

[111] Dermeik B, Lorenz H, Bonet A, Travitzky N (2019) Highly filled papers, on their manufacturing, processing, and applications. Adv Eng Mater 21:1900180. https://doi.org/10.1002/adem.201900180

[112] Pfeiffer S, Lorenz H, Fu Z, Fey T, Greil P, Travitzky N (2018) Al_2O_3/Cu-O composites fabricated by pressureless infiltration of paper-derived Al_2O_3 porous preforms. Ceram Int 44:20835–20840. https://doi.org/10.1016/j.ceramint.2018.08.087

[113] Schultheiß J, Dermeik B, Filbert-Demut I, Hock N, Yin X, Greil P, Travitzky N (2015) Processing and characterization of paper-derived Ti_3SiC_2 based ceramic. Ceram Int 41:12595–12603. https://doi.org/10.1016/j.ceramint.2015.06.085

[114] Lorenz H, Thäter J, Matias Carrijo MM, Rambo CR, Greil P, Travitzky N (2017) In situ synthesis of paper-derived Ti_3SiC_2. J Mater Res 32:3409–3414. https://doi.org/10.1557/jmr.2017.132

[115] Ge MN, Wang XF, Li GY, Lu C, Zhang JF, Tu R (2019) Synthesis of Cr_2AlC from elemental powders with modified pressureless spark plasma sintering. J Wuhan Univ Technol Mater Sci Edit 34:287–292. https://doi.org/10.1007/s11595-019-2048-4

[116] Li J, Guan L, Wang S, Cao J, Li X (2018) Research progress in flash sintering technology of ceramic materials. China Ceram Ind 25:20–26. https://doi.org/10.13958/j.cnki.ztcg.2018.06.005 **(in Chinese)**

[117] Karakuscu A, Cologna M, Yarotski D, Won J, Francis JSC, Raj R, Uberuaga BP (2012) Defect structure of flash-sintered strontium titanate. J Am Ceram Soc 95:2531–2536. https://doi.org/10.1111/j.1551-2916.2012.05240.x

[118] Muccillo R, Muccillo ENS (2014) Electric field-assisted flash sintering of tin dioxide. J Eur Ceram Soc 34:915–923. https://doi.org/10.1016/j.jeurceramsoc.2013.09.017

[119] Sun KN, Zhang J, Jiang TZ, Qiao JS, Sun W, Rooney D, Wang ZH (2016) Flash-sintering and characterization of La0.8Sr0.2Ga0.8Mg0.2O3-delta electrolytes for solid oxide fuel cells. Electrochim Acta 196:487–495. https://doi.org/10.1016/j.electacta.2016.02.207

[120] Fu Z, Ji W, Wang W (2017) Recent progress in flash sintering technology of ceramic materials. J Chin Ceram Soc 45:1211–1219. https://doi.org/10.14062/j.issn.0454-5648.2017.09.01 **(in Chinese)**

[121] Yu M, Grasso S, McKinnon R, Saunders T, Reece MJ (2017) Review of flash sintering: materials, mechanisms and modelling. Adv Appl Ceram 116:24–60. https://doi.org/10.1080/17436753.2016.1251051

[122] Grasso S, Saunders T, Porwal H, Cedillos-Barraza O, Jayaseelan DD, Lee WE, Reece MJ (2014) Flash spark plasma sintering (FSPS) of pure ZrB_2. J Am Ceram Soc 97:2405–2408. https://doi.org/10.1111/jace.13109

[123] Vasylkiv O, Borodianska H, Sakka Y, Demirskyi D (2016) Flash spark plasma sintering of ultrafine yttria-stabilized zirconia ceramics. Scr Mater 121:32–36. https://doi.org/10.1016/j.scriptamat.2016.04.031

[124] Grasso S, Saunders T, Porwal H, Milsom B, Tudball A, Reece M (2016) Flash spark plasma sintering (FSPS) of α and β SiC. J Am Ceram Soc 99:1534–1543. https://doi.org/10.1111/jace.14158

[125] Niu B, Zhang F, Zhang JY, Ji W, Wang WM, Fu ZY (2016) Ultra-fast densification of boron carbide by flash spark plasma sintering. Scr Mater 116:127–130. https://doi.org/10.1016/j.scriptamat.2016.02.012

[126] McKinnon R, Grasso S, Tudball A, Reece MJ (2017) Flash spark plsma sintering of cold-pressed TiB_2–hBN. J Eur Ceram Soc 37:2787–2794. https://doi.org/10.1016/j.jeurceramsoc.2017.01.029

[127] Grasso S, Saunders T, McKinnon R, Castle E, Tatarko P, Du BL, Gucci F, Yu M et al (2016) Spark plasma sintering in a flash. Am Ceram Soc Bull 95:32–34

[128] Cologna M, Rashkova B, Raj R (2010) Flash sintering of nanograin zirconia in < 5 s at 850 °C. J Am Ceram Soc 93:3556–3559. https://doi.org/10.1111/j.1551-2916.2010.04089.x

[129] M'Peko JC, Francis JSC, Raj R (2014) Field-assisted sintering of undoped $BaTiO_3$: microstructure evolution and dielectric permittivity. J Eur Ceram Soc 34:3655–3660. https://doi.org/10.1016/j.jeurceramsoc.2014.04.041

[130] Perez-Maqueda LA, Gil-Gonzalez E, Perejon A, Lebrun JM, Sanchez-Jimenez PE, Raj R (2017) Flash sintering of highly insulating nanostructured phase-pure $BiFeO_3$. J Am Ceram Soc 100:3365–3369. https://doi.org/10.1111/jace.14990

[131] Kok D, Jha SK, Raj R, Mecartney ML (2017) Flash sintering of a three-phase alumina, spinel, and yttria-stabilized zirconia composite. J Am Ceram Soc 100:3262–3268. https://doi.org/10.1111/jace.14818

[132] Bajpai I, Han YH, Yun J, Francis J, Kim S, Raj R (2016) Preliminary investigation of hydroxyapatite microstructures prepared by flash sintering. Adv Appl Ceram 115:276–281. https://doi.org/10.1080/17436753.2015.1136777

[133] Biesuz M, Luchi P, Quaranta A, Martucci A, Sglavo VM (2017) Photoemission during flash sintering: an interpretation based on thermal radiation. J Eur Ceram Soc 37:3125–3130. https://doi.org/10.1016/j.jeurceramsoc.2017.03.050

[134] Quach DV, Avila-Paredes H, Kim S, Martin M, Munir ZA (2010) Pressure effects and grain growth kinetics in the consolidation of nanostructured fully stabilized zirconia by pulsed electric current sintering. Acta Mater 58:5022–5030. https://doi.org/10.1016/j.actamat.2010.05.038

[135] Shen ZJ, Johnsson M, Zhao Z, Nygren M (2002) Spark plasma sintering of alumina. J Am Ceram Soc 85:1921–1927. https://doi.org/10.1111/j.1151-2916.2002.tb00381.x

[136] Schmerbauch C, Gonzalez-Julian J, Roder R, Ronning C, Guillon O (2014) Flash sintering of nanocrystalline zinc oxide and its influence on microstructure and defect formation. J Am Ceram Soc 97:1728–1735. https://doi.org/10.1111/jace.12972

[137] Ji W, Parker B, Falco S, Zhang JY, Fu ZY, Todd RI (2017) Ultra-fast firing: effect of heating rate on sintering of 3YSZ, with and without an electric field. J Eur Ceram Soc 37:2547–2551. https://doi.org/10.1016/j.jeurceramsoc.2017.01.033

[138] Cologna M, Raj R (2011) Surface diffusion-controlled neck growth kinetics in early stage sintering of zirconia, with and without applied DC electrical field. J Am Ceram Soc 94:391–395. https://doi.org/10.1111/j.1551-2916.2010.04088.x

[139] Schie M, Menzel S, Robertson J, Waser R, De Souza RA (2018) Field-enhanced route to generating anti-Frenkel pairs in HfO_2. Phys Rev Mater 2:035002. https://doi.org/10.1103/PhysRevMaterials.2.035002

[140] Genreith-Schriever AR, De Souza RA (2016) Field-enhanced ion transport in solids: reexamination with molecular dynamics simulations. Phys Rev B 94:224304. https://doi.org/10.1103/PhysRevB.94.224304

[141] Sankaranarayanan S, Kaxiras E, Ramanathan S (2009) Electric field tuning of oxygen stoichiometry at oxide surfaces: molecular dynamics simulations studies of zirconia. Energy Environ Sci 2:1196–1204. https://doi.org/10.1039/b913154j

[142] Koniuszewska A, Naplocha K (2016) Microwave assisted self-propagating high-temperature synthesis of Ti_2AlC max phase. Compos Theory Pract 16:109–112

[143] Hamm CM, Schafer T, Zhang HB, Birkel CS (2016) Non-conventional Synthesis of the 413 MAX Phase V_4AlC_3. Z Anorg Allg Chem 642:1397–1401. https://doi.org/10.1002/zaac.201600370

[144] Xie M-y, Shi J-j, Chen G-p, Li X (2019) Research progress and prospect of microwave sintering technology. Powder Metall Ind 29:66–72. https://doi.org/10.13228/j.boyuan.issn1006-6543.20180019 **(in Chinese)**

[145] Zhang H, Wang X-H, Zhou Y-C (2019) Crystal defects in MAX phases: the current status and future directions. Adv Ceram 40:150–173. https://doi.org/10.16253/j.cnki.37-1226/tq.2019.03.002 **(in Chinese)**

[146] Li CL, Wang ZQ, Ma DC, Wang CY, Wang BL (2013) First-principles study of the structural, mechanical, magnetic, and electronic properties of Cr_4AlN_3 under pressure. Intermetallics 43:71–78. https://doi.org/10.1016/j.intermet.2013.07.015

[147] Barsoum MW, Radovic M (2011) Elastic and mechanical properties of the MAX phases. Ann Rev Mater Res

41:195–227. https://doi.org/10.1146/annurev-matsci-062910-100448

[148] Khazaei M, Arai M, Sasaki T, Estili M, Sakka Y (2014) The effect of the interlayer element on the exfoliation of layered Mo(2)AC (A = Al, Si, P, Ga, Ge, As or In) MAX phases into two-dimensional Mo_2C nanosheets. Sci Technol Adv Mater 15:014208. https://doi.org/10.1088/1468-6996/15/1/014208

[149] Sun ZM, Hashimoto H, Tian WB, Zou Y (2010) Synthesis of the MAX phases by pulse discharge sintering. Int J Appl Ceram Technol 7:704–718. https://doi.org/10.1111/j.1744-7402.2010.02555.x

[150] Hossein-Zadeh M, Mirzaee O, Mohammadian-Semnani H (2019) An investigation into the microstructure and mechanical properties of V_4AlC_3 MAX phase prepared by spark plasma sintering. Ceram Int 45:7446–7457. https://doi.org/10.1016/j.ceramint.2019.01.036

[151] Bazhin PM, Stel'makh LS, Stolin AM (2019) Effect of strain on the formation of a MAX Phase in Ti–Al–C materials during self-propagating high temperature synthesis and extrusion. Inorg Mater 55:302–307. https://doi.org/10.1134/s0020168519030051

[152] Istomina EI, Istomin PV, Nadutkin AV, Grass VE, Bogdanova AS (2018) Optimization of the carbosilicothermic synthesis of the Ti_4SiC_3 MAX phase. Inorg Mater 54:528–536. https://doi.org/10.1134/s0020168518060055

[153] He RJ, Cheng XM, Qu ZL, Fang DN (2016) Pull-off behavior of MAX phase ceramic bolted connections: experimental testing and simulation analysis. Adv Eng Mater 18:591–596. https://doi.org/10.1002/adem.201500288

[154] Mashtalir O, Naguib M, Mochalin VN, Dall'Agnese Y, Heon M, Barsoum MW, Gogotsi Y (2013) Intercalation and delamination of layered carbides and carbonitrides. Nat Commun 4:1716. https://doi.org/10.1038/ncomms2664

[155] Son W, Duong T, Talapatra A, Prehn E, Tan ZY, Radovic M, Arroyave R (2018) Minimal effect of stacking number on intrinsic cleavage and shear behavior of Tin + 1AlCn and Tan + 1AlCn MAX phases. J Appl Phys 123:225102. https://doi.org/10.1063/1.5026323

[156] Lin ZJ, Zhuo MJ, Zhou YC, Li MS, Wang JY (2006) Microstructures and theoretical bulk modulus of layered ternary tantalum aluminum carbides. J Am Ceram Soc 89:3765–3769. https://doi.org/10.1111/j.1551-2916.2006.01303.x

[157] Zhang J, Liu B, Wang JY, Zhou YC (2009) Low-temperature instability of Ti_2SnC: a combined transmission electron microscopy, differential scanning calorimetry, and X-ray diffraction investigations. J Mater Res 24:39–49. https://doi.org/10.1557/jmr.2009.0012

[158] Hamm CM, Durrschnabel M, Molina-Luna L, Salikhov R, Spoddig D, Farle M, Wiedwald U, Birkel CS (2018) Structural, magnetic and electrical transport properties of non-conventionally prepared MAX phases V_2AlC and (V/Mn)(2)AlC. Mater Chem Front 2:483–490. https://doi.org/10.1039/c7qm00488e

[159] Liu ZM, Zheng LY, Sun LC, Qian YH, Wang JY, Li MS (2014) (Cr2/3Ti1/3)(3)AlC2 and (Cr5/8Ti3/8)(4)AlC3: new MAX-phase compounds in Ti–Cr–Al–C system. J Am Ceram Soc 97:67–69. https://doi.org/10.1111/jace.12731

[160] Wan DT, He LF, Zheng LL, Zhang J, Bao YW, Zhou YC (2010) A new method to improve the high-temperature mechanical properties of Ti_3SiC_2 by substituting Ti with Zr, Hf, or Nb. J Am Ceram Soc 93:1749–1753. https://doi.org/10.1111/j.1551-2916.2010.03637.x

[161] Tian WB, Sun ZM, Hashimoto H, Du YL (2009) Synthesis, microstructure and properties of (Cr1-xVx)(2)AlC solid solutions. J Alloys Compd 484:130–133. https://doi.org/10.1016/j.jallcom.2009.04.111

[162] Meng FL, Zhou YC, Wang JY (2005) Strengthening of Ti_2AlC by substituting Ti with V. Scr Mater 53:1369–1372. https://doi.org/10.1016/j.scriptamat.2005.08.030

[163] Talapatra A, Duong T, Son W, Gao H, Radovic M, Arroyave R (2016) High-throughput combinatorial study of the effect of M site alloying on the solid solution behavior of M2AlC MAX phases. Phys Rev B 94:104106. https://doi.org/10.1103/PhysRevB.94.104106

[164] Naguib M, Bentzel GW, Shah J, Halim J, Caspi EN, Lu J, Hultman L, Barsoum MW (2014) New solid solution MAX phases: (Ti-0.5, V-0.5)(3)AlC2, (Nb-0.5, V0.5)(2)AlC, (Nb-0.5, V-0.5)(4)AlC3 and (Nb-0.8, Zr-0.2)(2)AlC. Mater Res Lett 2:233–240. https://doi.org/10.1080/21663831.2014.932858

[165] Sobolev KV, Kolincio KK, Emelyanov A, Mielewczyk-Gryn A, Gazda M, Roman M, Pazniak A, Rodionova V (2020) Evolution of magnetic and transport properties in (Cr1–xMnx)(2)AlC MAX-phase synthesized by arc melting technique. J Magn Magn Mater 493:165642. https://doi.org/10.1016/j.jmmm.2019.165642

[166] Konovalikhin SV, Guda SA, Kovalev DY (2018) Composition and structure of (Zr0.37Ti0.63)(3)AlC2 MAX phase crystals prepared by self-propagating high-temperature synthesis. Inorg Mater 54:953–956. https://doi.org/10.1134/s0020168518090054

[167] Horlait D, Middleburgh SC, Chroneos A, Lee WE (2016) Synthesis and DFT investigation of new bismuth-containing MAX phases. Sci Rep 6:18829. https://doi.org/10.1038/srep18829

[168] Nechiche M, Cabioc'h T, Casp EN, Rivin O, Hoser A, Gauthier-Brunet V, Chartier P, Dubois S (2017) Evidence

for symmetry reduction in Ti-3(Al1-delta Cu delta)C-2 MAX phase solid solutions. Inorg Chem 56:14388–14395. https://doi.org/10.1021/acs.inorgchem.7b01003

[169] Zhou YC, Chen JX, Wang JY (2006) Strengthening of Ti_3AlC_2 by incorporation of Si to form Ti3Al1–xSixC2 solid solutions. Acta Mater 54:1317–1322. https://doi.org/10.1016/j.actamat.2005.10.057

[170] Arroyave R, Talapatra A, Duong T, Son W, Gao H, Radovic M (2017) Does aluminum play well with others? Intrinsic Al–A alloying behavior in 211/312 MAX phases. Mater Res Lett 5:170–178. https://doi.org/10.1080/21663831.2016.1241319

[171] Horlait D, Grasso S, Chroneos A, Lee WE (2016) Attempts to synthesise quaternary MAX phases (Zr, M)(2)AlC and Zr-2(Al, A)C as a way to approach Zr_2AlC. Mater Res Lett 4:137–144. https://doi.org/10.1080/21663831.2016.1143053

[172] Xu XL, Ngai TL, Li YY (2015) Synthesis and characterization of quarternary Ti3Si(1-x)AlxC2 MAX phase materials. Ceram Int 41:7626–7631. https://doi.org/10.1016/j.ceramint.2015.02.088

[173] Jiang C, Chroneos A (2018) Ab initio modeling of MAX phase solid solutions using the special quasirandom structure approach. Phys Chem Chem Phys 20:1173–1180. https://doi.org/10.1039/c7cp07576f

[174] Lapauw T, Tunca B, Potashnikov D, Pesach A, Ozeri O, Vleugels J, Lambrinou K (2018) The double solid solution (Zr, Nb)(2)(Al, Sn)C MAX phase: a steric stability approach. Sci Rep 8:12801. https://doi.org/10.1038/s41598-018-31271-2

[175] Nechiche M, Gauthier-Brunet V, Mauchamp V, Joulain A, Cabioc'h T, Milhet X, Chartier P, Dubois S (2017) Synthesis and characterization of a new (Ti1-epsilon, Cu-epsilon)(3)(Al, Cu)C-2 MAX phase solid solution. J Eur Ceram Soc 37:459–466. https://doi.org/10.1016/j.jeurceramsoc.2016.09.028

[176] Griseri M, Tunca B, Huang SG, Dahlqvist M, Rosen J, Lu J, Persson POA, Popescu L et al (2020) Ta-based 413 and 211 MAX phase solid solutions with Hf and Nb. J Eur Ceram Soc 40:1829–1838. https://doi.org/10.1016/j.jeurceramsoc.2019.12.052

[177] Tunca B, Lapauw T, Karakulina OM, Batuk M, Cabioc'h T, Hadermann J, Delville R, Lambrinou K et al (2017) Synthesis of MAX phases in the Zr–Ti–Al–C system. Inorg Chem 56:3489–3498. https://doi.org/10.1021/acs.inorgchem.6b03057

[178] Halim J, Palisaitis J, Lu J, Thornberg J, Moon EJ, Precner M, Eklund P, Persson POA et al (2018) Synthesis of two-dimensional Nb1.33C (MXene) with randomly distributed vacancies by etching of the quaternary solid solution (Nb2/3Sc1/3)(2)AIC MAX phase. ACS Appl Nano Mater 1:2455–2460. https://doi.org/10.1021/acsanm.8b00332

[179] Dubois S, Bei GP, Tromas C, Gauthier-Brunet V, Gadaud P (2010) Synthesis, microstructure, and mechanical properties of Ti3Sn(1-x)AlxC2 MAX phase solid solutions. Int J Appl Ceram Technol 7:719–729. https://doi.org/10.1111/j.1744-7402.2010.02554.x

[180] Yu WB, Li SB, Sloof WG (2010) Microstructure and mechanical properties of a $Cr_2Al(Si)C$ solid solution. Mater Sci Eng A Struct Mater Prop Microstruct Process 527:5997–6001. https://doi.org/10.1016/j.msea.2010.05.093

[181] Dahlqvist M, Lu J, Meshkian R, Tao QZ, Hultman L, Rosen J (2017) Prediction and synthesis of a family of atomic laminate phases with Kagome-like and in-plane chemical ordering. Sci Adv 3:e1700642. https://doi.org/10.1126/sciadv.1700642

[182] Meshkian R, Tao QZ, Dahlqvist M, Lu J, Hultman L, Rosen J (2017) Theoretical stability and materials synthesis of a chemically ordered MAX phase, Mo_2ScAlC_2, and its two-dimensional derivate Mo_2ScC_2 MXene. Acta Mater 125:476–480. https://doi.org/10.1016/j.actamat.2016.12.008

[183] Meshkian R, Dahlqvist M, Lu J, Wickman B, Halim J, Thornberg J, Tao QZ, Li SX et al (2018) W-based atomic laminates and their 2D derivative W1.33C MXene with vacancy ordering. Adv Mater 30:1706409. https://doi.org/10.1002/adma.201706409

[184] Lu J, Thore A, Meshkian R, Tao Q, Hultman L, Rosen J (2017) Theoretical and experimental exploration of a novel in-plane chemically ordered (Cr2/3M1/3)(2)AIC i-MAX Phase with M = Sc and Y. Cryst Growth Des 17:5704–5711. https://doi.org/10.1021/acs.cgd.7b00642

[185] Petruhins A, Dahlqvist M, Lu J, Hultman L, Rosen J (2020) Theoretical prediction and experimental verification of the chemically ordered atomic-laminate i-MAX phases (Cr2/3Sc1/3)(2)GaC and (Mn2/3Sc1/3)(2)GaC. Cryst Growth Des 20:55–61. https://doi.org/10.1021/acs.cgd.9b00449

[186] Tao QZ, Dahlqvist M, Lu J, Kota S, Meshkian R, Halim J, Palisaitis J, Hultman L et al (2017) Two-dimensional Mo1.33C MXene with divacancy ordering prepared from parent 3D laminate with in-plane chemical ordering. Nat Commun 8:14949. https://doi.org/10.1038/ncomms14949

[187] Liu ZM, Wu ED, Wang JM, Qian YH, Xiang HM, Li XC, Jin QQ, Sun GG et al (2014) Crystal structure and formation mechanism of (Cr2/3Ti1/3)(3)A1C(2) MAX phase. Acta Mater 73:186–193. https://doi.org/10.1016/j.actamat.2014.04.006

[188] Anasori B, Halim J, Lu J, Voigt CA, Hultman L, Barsoum MW (2015) Mo_2TiAlC_2: a new ordered layered ternary

carbide. Scr Mater 101:5–7. https://doi.org/10.1016/j.scriptamat.2014.12.024

[189] Thornberg J, Halim J, Lu J, Meshkian R, Palisaitis J, Hultman L, Persson POA, Rosen J (2019) Synthesis of (V2/3Sc1/3)(2)AlC i-MAX phase and V2-xC MXene scrolls. Nanoscale 11:14720–14726. https://doi.org/10.1039/c9nr02354b

[190] Persson I, el Ghazaly A, Tao QZ, Halim J, Kota S, Darakchieva V, Palisaitis J, Barsoum MW et al (2018) Tailoring structure, composition, and energy storage properties of MXenes from selective etching of in-plane, chemically ordered MAX phases. Small 14:1703676. https://doi.org/10.1002/smll.201703676

[191] Mockute A, Tao Q, Dahlqvist M, Lu J, Calder S, Caspi EN, Hultman L, Rosen J (2019) Materials synthesis, neutron powder diffraction, and first-principles calculations of (MoxSc1-x)(2)AlC i-MAX phase used as parent material for MXene derivation. Phys Rev Mater 3:113607. https://doi.org/10.1103/PhysRevMaterials.3.113607

[192] Zhang H, Wang XH, Ma YH, Sun LC, Zheng LY, Zhou YC (2012) Crystal structure determination of nanolaminated $Ti_5Al_2C_3$ by combined techniques of XRPD, TEM and ab initio calculations. J Adv Ceram 1:268–273. https://doi.org/10.1007/s40145-012-0034-9

[193] Wang XH, Zhang H, Zheng LY, Ma YH, Lu XP, Sun YJ, Zhou YC (2012) $Ti_5Al_2C_3$: a new ternary carbide belonging to MAX phases in the Ti–Al–C system. J Am Ceram Soc 95:1508–1510. https://doi.org/10.1111/j.1551-2916.2012.05158.x

[194] Wilhelmsson O, Palmquist JP, Lewin E, Emmerlich J, Eklund P, Persson POA, Hogberg H, Li S et al (2006) Deposition and characterization of ternary thin films within the Ti–Al–C system by DC magnetron sputtering. J Cryst Growth 291:290–300. https://doi.org/10.1016/j.jcrysgro.2006.03.008

[195] Lane NJ, Naguib M, Lu J, Hultman L, Barsoum MW (2012) Structure of a new bulk $Ti_5Al_2C_3$ MAX phase produced by the topotactic transformation of Ti_2AlC. J Eur Ceram Soc 32:3485–3491. https://doi.org/10.1016/j.jeurceramsoc.2012.03.035

[196] Zhou YC, Meng FL, Zhang J (2008) New MAX-phase compounds in the V–Cr–Al–C system. J Am Ceram Soc 91:1357–1360. https://doi.org/10.1111/j.1551-2916.2008.02279.x

[197] Palmquist JP, Li S, Persson POA, Emmerlich J, Wilhelmsson O, Hogberg H, Katsnelson MI, Johansson B et al (2004) M(n + 1)AX(n) phases in the Ti–Si–C system studied by thin-film synthesis and ab initio calculations. Phys Rev B 70:165401. https://doi.org/10.1103/PhysRevB.70.165401

[198] Högberg H, Eklund P, Emmerlich J, Birch J, Hultman L (2005) Epitaxial Ti_2GeC, Ti_3GeC_2, and Ti_4GeC_3 MAX-phase thin films grown by magnetron sputtering. J Mater Res 20:779–782. https://doi.org/10.1557/JMR.2005.0105

[199] Lapauw T, Tunca B, Cabioc'h T, Lu J, Persson POA, Lambrinou K, Vleugels J (2016) Synthesis of MAX Phases in the Hf–Al–C System. Inorg Chem 55:10922–10927. https://doi.org/10.1021/acs.inorgchem.6b01398

[200] Scabarozi TH, Hettinger JD, Lofland SE, Lu J, Hultman L, Jensen J, Eklund P (2011) Epitaxial growth and electrical-transport properties of $Ti_7Si_2C_5$ thin films synthesized by reactive sputter-deposition. Scr Mater 65:811–814. https://doi.org/10.1016/j.scriptamat.2011.07.038

[201] Hu C, Lai CC, Tao Q, Lu J, Halim J, Sun L, Zhang J, Yang J et al (2015) Mo_2Ga_2C: a new ternary nanolaminated carbide. Chem Commun 51:6560–6563. https://doi.org/10.1039/c5cc00980d

[202] Jin S, Wang ZT, Du YQ, Hu QK, Yu JG, Zhou AG (2020) Hot-pressing sintering of double-a-layer MAX phase Mo_2Ga_2C. J Inorg Mater 35:41–45. https://doi.org/10.15541/jim20190296

[203] Fashandi H, Lai CC, Dahlqvist M, Lu J, Rosen J, Hultman L, Greczynski G, Andersson M et al (2017) Ti_2Au_2C and $Ti_3Au_2C_2$ formed by solid state reaction of gold with Ti_2AlC and Ti_3AlC_2. Chem Commun 53:9554–9557. https://doi.org/10.1039/c7cc04701k

[204] Chen HX, Yang DL, Zhang QH, Jin SF, Guo LW, Deng J, Li XD, Chen XL (2019) A series of MAX phases with MA-triangular-prism bilayers and elastic properties. Angew Chem-Int Edit 58:4576–4580. https://doi.org/10.1002/anie.201814128

[205] Zhang H, Hu T, Wang XH, Li ZJ, Hu MM, Wu ED, Zhou YC (2015) Discovery of carbon-vacancy ordering in Nb_4AlC_3-x under the guidance of first-principles calculations. Sci Rep 5:14192. https://doi.org/10.1038/srep14192

[206] Etzkorn J, Ade M, Hillebrecht H (2007) V2AlC, V4AlC3-x (x approximate to 0.31), and V12Al3C8: synthesis, crystal growth, structure, and superstructure. Inorg Chem 46:7646–7653. https://doi.org/10.1021/ic700382y

[207] Ashton M, Hennig RG, Broderick SR, Rajan K, Sinnott SB (2016) Computational discovery of stable M(2)AX phases. Phys Rev B 94:054116. https://doi.org/10.1103/PhysRevB.94.054116

[208] Anasori B, Dahlqvist M, Halim J, Moon EJ, Lu J, Hosler BC, Caspi EN, May SJ et al (2015) Experimental and theoretical characterization of ordered MAX phases Mo_2TiAlC_2 and $Mo_2Ti_2AlC_3$. J Appl Phys 118:094304. https://doi.org/10.1063/1.4929640

[209] Dahlqvist M, Rosen J (2020) Predictive theoretical screening of phase stability for chemical order and disorder

in quaternary 312 and 413 MAX phases. Nanoscale 12:785–794. https://doi.org/10.1039/c9nr08675g

[210] Konovalikhin SV, Mingazov AI, Guda SA, Kovalev DY (2019) Estimating the stability of the structure of MAX phases of Ti3AlC2-xBx composition on the basis of quantum-chemical calculations. Russ J Phys Chem A 93:1277–1280. https://doi.org/10.1134/s0036024419070112

[211] Burr PA, Horlait D, Lee WE (2017) Experimental and DFT investigation of (Cr, Ti)(3)AlC2 MAX phases stability. Mater Res Lett 5:144–157. https://doi.org/10.1080/21663831.2016.1222598

[212] Chen LL, Deng ZX, Li M, Li P, Chang KK, Huang F, Du SY, Huang Q (2020) Phase diagrams of Novel MAX phases. J Inorg Mater 35:35–40. https://doi.org/10.15541/jim20190184

[213] Hossein-Zadeh M, Mirzaee O, Mohammadian-Semnani H, Razavi M (2019) Microstructure investigation of V2AlC MAX phase synthesized through spark plasma sintering using two various sources V and V_2O_5 as the starting materials. Ceram Int 45:23902–23916. https://doi.org/10.1016/j.ceramint.2019.07.236

[214] Scheibe B, Kupka V, Peplinska B, Jarek M, Tadyszak K (2019) the influence of oxygen concentration during MAX phases (Ti_3AlC_2) preparation on the $-Al_2O_3$ microparticles content and specific surface area of multilayered MXenes ($Ti_3C_2T_x$). Materials 12:353. https://doi.org/10.3390/ma12030353

[215] Duan XM, Shen L, Jia DC, Zhou Y, van der Zwaag S, Sloof WG (2015) Synthesis of high-purity, isotropic or textured Cr_2AlC bulk ceramics by spark plasma sintering of pressure-less sintered powders. J Eur Ceram Soc 35:1393–1400. https://doi.org/10.1016/j.jeurceramsoc.2014.11.008

[216] Gorshkov VA, Miloserdov PA, Karpov AV, Shchukin AS, Sytschev AE (2019) Investigation of the composition and properties of a Cr_2AlC MAX phase-based material prepared by metallothermic SHS. Phys Met Metallogr 120:471–475. https://doi.org/10.1134/s0031918x19050041

[217] Akhlaghi M, Tayebifard SA, Salahi E, Asl MS, Schmidt G (2018) Self-propagating high-temperature synthesis of Ti_3AlC_2 MAX phase from mechanically-activated Ti/Al/graphite powder mixture. Ceram Int 44:9671–9678. https://doi.org/10.1016/j.ceramint.2018.02.195

[218] Hu CF, Zhang J, Bao YW, Wang JY, Li MS, Zhou YC (2008) In-situ reaction synthesis and decomposition of Ta_2AlC. Int J Mater Res 99:8–13. https://doi.org/10.3139/146.101598

[219] Hu CF, He LF, Liu MY, Wang XH, Wang JY, Li MS, Bao YW, Zhou YC (2008) in situ reaction synthesis and mechanical properties of V_2AlC. J Am Ceram Soc 91:4029–4035. https://doi.org/10.1111/j.1551-2916.2008.02774.x

[220] Hasegawa G, Kawahara K, Shima K, Inada M, Enomoto N, Hayashi K (2019) Characterization of an AX compound derived from Ti_2SC MAX phase. Eur J Inorg Chem 2019:2312–2317. https://doi.org/10.1002/ejic.201900311

[221] Bei GP, Gauthier-Brunet V, Tromas C, Dubois S (2012) Synthesis, characterization, and intrinsic hardness of layered nanolaminate Ti_3AlC_2 and Ti3Al0.8Sn0.2C2 solid solution. J Am Ceram Soc 95:102–107. https://doi.org/10.1111/j.1551-2916.2011.04846.x

[222] Tian W, Vanmeensel K, Wang P, Zhang G, Li Y, Vleugels J, Van der Biest O (2007) Synthesis and characterization of Cr_2AlC ceramics prepared by spark plasma sintering. Mater Lett 61:4442–4445. https://doi.org/10.1016/j.matlet.2007.02.023

[223] Kozak K, Bucko MM, Chlubny L, Lis J, Antou G, Chotard T (2019) Influence of composition and grain size on the damage evolution in MAX phases investigated by acoustic emission. Mater Sci Eng A Struct Mater Prop Microstruct Process 743:114–122. https://doi.org/10.1016/j.msea.2018.11.063

[224] Hu C, Sakka Y, Grasso S, Nishimura T, Guo S, Tanaka H (2011) Shell-like nanolayered Nb_4AlC_3 ceramic with high strength and toughness. Scr Mater 64:765–768. https://doi.org/10.1016/j.scriptamat.2010.12.045

[225] Parrikar PN, Benitez R, Gao H, Radovic M, Shukla A (2017) The effect of grain size on deformation and failure of Ti_2AlC MAX phase under thermo-mechanical loading. Exp Mech 57:675–685. https://doi.org/10.1007/s11340-017-0264-4

[226] Griseri M, Tunca B, Lapauw T, Huang SG, Popescu L, Barsoum MW, Lambrinou K, Vleugels J (2019) Synthesis, properties and thermal decomposition of the Ta_4AlC_3 MAX phase. J Eur Ceram Soc 39:2973–2981. https://doi.org/10.1016/j.jeurceramsoc.2019.04.021

[227] Sun ZM (2013) Progress in research and development on MAX phases: a family of layered ternary compounds. Int Mater Rev 56:143–166. https://doi.org/10.1179/1743280410y.0000000001

[228] Gilbert CJ, Bloyer DR, Barsoum MW, El-Raghy T, Tomsia AP, Ritchie RO (2000) Fatigue-crack growth and fracture properties of coarse and fine-grained Ti_3SiC_2. Scr Mater 42:761–767. https://doi.org/10.1016/S1359-6462(99)00427-3

[229] Sun ZM, Murugaiah A, Zhen T, Zhou A, Barsoum MW (2005) Microstructure and mechanical properties of porous Ti_3SiC_2. Acta Mater 53:4359–4366. https://doi.org/10.1016/j.actamat.2005.05.034

[230] Radovic M, Barsoum MW, El-Raghy T, Wiederhorn SM, Luecke WE (2002) Effect of temperature, strain rate and grain size on the mechanical response of Ti_3SiC_2 in tension. Acta Mater 50:1297–1306. https://doi.org/10.1016/S1359-6454(01)00424-4

[231] El-Raghy T, Barsoum MW, Zavaliangos A, Kalidindi SR (1999) Processing and mechanical properties of Ti_3SiC_2: II, effect of grain size and deformation temperature. J Am Ceram Soc 82:2855–2860. https://doi.org/10.1111/j.1151-2916.1999.tb02167.x

[232] Fraczkiewicz M, Zhou AG, Barsoum MW (2006) Mechanical damping in porous Ti_3SiC_2. Acta Mater 54:5261–5270. https://doi.org/10.1016/j.actamat.2006.06.052

[233] Parrikar PN, Benitez R, Radovic M, Shukla A (2017) Effect of microstructure on mechanical response of MAX phases. In: Ralph WC, Singh R, Tandon G, Thakre PR, Zavattieri P, Zhu Y (eds) Mechanics of composite and multi-functional materials. Springer, Berlin, pp 171–175

[234] Lapauw T, Swarnakar AK, Tunca B, Lambrinou K, Vleugels J (2018) Nanolaminated ternary carbide (MAX phase) materials for high temperature applications. Int J Refract Met Hard Mater 72:51–55. https://doi.org/10.1016/j.ijrmhm.2017.11.038

[235] Radovic M, Barsoum MW, El-Raghy T, Wiederhorn SM (2003) Tensile creep of coarse-grained Ti_3SiC_2 in the 1000–1200 °C temperature range. J Alloys Compd 361:299–312. https://doi.org/10.1016/s0925-8388(03)00435-3

[236] Radovic M, Barsoum MW, El-Raghy T, Wiederhorn S (2001) Tensile creep of fine grained (3–5 μm) Ti_3SiC_2 in the 1000–1200 °C temperature range. Acta Mater 49:4103–4112. https://doi.org/10.1016/S1359-6454(01)00243-9

[237] Wan DT, Zhou YC, Bao YW, Yan CK (2006) In situ reaction synthesis and characterization of Ti3Si(Al)C-2/SiC composites. Ceram Int 32:883–890. https://doi.org/10.1016/j.ceramint.2005.07.004

[238] Salvo C, Chicardi E, Garcia-Garrido C, Jimenez JA, Aguilar C, Usuba J, Mangalaraja RV (2019) The influence of mechanical activation process on the microstructure and mechanical properties of bulk Ti_2AlN MAX phase obtained by reactive hot pressing. Ceram Int 45:17793–17799. https://doi.org/10.1016/j.ceramint.2019.05.350

[239] Song GM, Xu Q, Sloof WG, Li SB, Svd Zwaag (2009) Toughening of a ZrC particle-reinforced Ti_3AIC_2 composite. In: Ohji T, Wereszczak A (eds) Mechanical properties and processing of ceramic binary, ternary, and composite systems: ceramic engineering and science proceedings, vol 29. Wiley, New York, pp 31–39

[240] Yang J, Pan L, Gu W, Qiu T, Zhang Y, Zhu S (2012) Microstructure and mechanical properties of in situ synthesized (TiB_2 + TiC)/Ti_3SiC_2 composites. Ceram Int 38:649–655. https://doi.org/10.1016/j.ceramint.2011.06.066

[241] Peng LM (2007) Preparation and properties of ternary Ti_3AlC_2 and its composites from Ti–Al–C powder mixtures with ceramic particulates. J Am Ceram Soc 90:1312–1314. https://doi.org/10.1111/j.1551-2916.2007.01517.x

[242] Pan W, Shi SL (2007) Microstructure and mechanical properties of Ti3SiC2/3Y-TZP composites by spark plasma sintering. J Eur Ceram Soc 27:413–417. https://doi.org/10.1016/j.jeurceramsoc.2006.05.072

[243] Chen XH, Bei GP (2017) toughening mechanisms in nanolayered MAX phase ceramics—a review. Materials 10:366. https://doi.org/10.3390/ma10040366

[244] Hu CF, Sakka Y, Grasso S, Suzuki T, Tanaka H (2011) Tailoring Ti_3SiC_2 ceramic via a strong magnetic field alignment method followed by spark plasma sintering. J Am Ceram Soc 94:742–748. https://doi.org/10.1111/j.1551-2916.2010.04186.x

[245] Lapauw T, Vanmeensel K, Lambrinou K, Vleugels J (2016) A new method to texture dense Mn + 1AXn ceramics by spark plasma deformation. Scr Mater 111:98–101. https://doi.org/10.1016/j.scriptamat.2015.08.023

[246] Sato K, Mishra M, Hirano H, Suzuki TS, Sakka Y (2014) Fabrication of textured Ti_3SiC_2 ceramic by slip casting in a strong magnetic field and pressureless sintering. J Ceram Soc Jpn 122:817–821. https://doi.org/10.2109/jcersj2.122.817

[247] Hu CF, Sakka Y, Tanaka H, Nishimura T, Grasso S (2011) Fabrication of textured Nb_4AlC_3 ceramic by slip casting in a strong magnetic field and spark plasma sintering. J Am Ceram Soc 94:410–415. https://doi.org/10.1111/j.1551-2916.2010.04096.x

[248] Zhang HB, Hu CF, Sato K, Grasso S, Estili M, Guo SQ, Morita K, Yoshida H et al (2015) Tailoring Ti_3AlC_2 ceramic with high anisotropic physical and mechanical properties. J Eur Ceram Soc 35:393–397. https://doi.org/10.1016/j.jeurceramsoc.2014.08.026

[249] El-Raghy T, Blau P, Barsoum MW (2000) Effect of grain size on friction and wear behavior of Ti_3SiC_2. Wear 238:125–130. https://doi.org/10.1016/S0043-1648(99)00348-8

[250] (2014) Summary of MAX phase synthesis conditions. https://wenku.baidu.com/view/e343763652ea551810a68790.html. Accessed 4 Jan 2014 **(in Chinese)**

[251] Chen ZW, Li ZY, Li JJ, Liu CB, Lao CS, Fu YL, Liu CY, Li Y et al (2019) 3D printing of ceramics: a review. J Eur

Ceram Soc 39:661–687. https://doi.org/10.1016/j.jeurceramsoc.2018.11.013

[252] Krinitcyn M, Fu ZW, Harris J, Kostikov K, Pribytkov GA, Greil P, Travitzky N (2017) laminated object manufacturing of in situ synthesized MAX-phase composites. Ceram Int 43:9241–9245. https://doi.org/10.1016/j.ceramint.2017.04.079

[253] Carrijo MMM, Lorenz H, Filbert-Demut I, Barra G, Hotza D, Yin XW, Greil P, Travitzky N (2016) Fabrication of Ti_3SiC_2-based composites via three-dimensional printing: Influence of processing on the final properties. Ceram Int 42:9557–9564. https://doi.org/10.1016/j.ceramint.2016.03.036

[254] Dermeik B, Travitzky N (2020) Laminated object manufacturing of ceramic-based materials. Adv Eng Mater. https://doi.org/10.1002/adem.202000256

[255] Spencer CB (2010) Fiber-reinforced Ti_3SiC_2 and Ti_2AlC mAX phase composites. Master Dissertation, Drexel University

[256] Spencer CB, Cordoba JM, Obando N, Sakulich A, Radovic M, Oden M, Hultman L, Barsoum MW (2011) Phase evaluation in Al_2O_3 fiber-reinforced Ti_2AlC during sintering in the 1300 °C–1500 °C temperature range. J Am Ceram Soc 94:3327–3334. https://doi.org/10.1111/j.1551-2916.2011.04612.x

[257] Lagos MA, Pellegrini C, Agote I, Azurmendi N, Barcena J, Parco M, Silvestroni L, Zoli L et al (2019) Ti_3SiC_2–Cf composites by spark plasma sintering: processing, microstructure and thermo-mechanical properties. J Eur Ceram Soc 39:2824–2830. https://doi.org/10.1016/j.jeurceramsoc.2019.03.037

[258] Naik Parrikar P, Gao H, Radovic M, Shukla A (2015) Static and dynamic thermo-mechanical behavior of Ti_2AlC MAX phase and fiber reinforced Ti_2AlC Composites. In: Song B, Casem D, Kimberley J (eds) dynamic behavior of materials, volume 1, conference proceedings of the society for experimental mechanics series. Springer, Berlin, pp 9–14

[259] Li K, Kashkarov E, Syrtanov M, Sedanova E, Ivashutenko A, Lider A, Fan P, Yuan DQ et al (2020) Preceramic paper-derived SiCf/SiCp composites obtained by spark plasma sintering: processing, microstruct mechanical properties. Materials 13:607. https://doi.org/10.3390/ma13030607

[260] Guo SQ (2016) Improvement of mechanical properties of SiC(SCS-6) fibre-reinforced Ti_3AlC_2 matrix composites with Ti barrier layer. J Eur Ceram Soc 36:1349–1358. https://doi.org/10.1016/j.jeurceramsoc.2015.12.039

[261] Guo SQ, Hu CF, Gao H, Tanaka Y, Kagawa Y (2015) SiC(SCS-6) fiber-reinforced Ti_3AlC_2 matrix composites: interfacial characterization and mechanical behavior. J Eur Ceram Soc 35:1375–1384. https://doi.org/10.1016/j.jeurceramsoc.2014.11.034

[262] Zoli L, Vinci A, Silvestroni L, Sciti D, Reece M, Grasso S (2017) Rapid spark plasma sintering to produce dense UHTCs reinforced with undamaged carbon fibres. Mater Des 130:1–7. https://doi.org/10.1016/j.matdes.2017.05.029